000

255001

SCINTREX

COMMENTS ON

FURTHER ELECTRICAL INDUCED POLARIZATION SURVEYS

OVER THE BOCO GRID, NEAR ROSEBERY, TASMANIA

ON BEHALF OF

ELECTROLYTIC ZINC COMPANY OF AUSTRALASIA LIMITED

E.L. 12/72.

001

255002

SCINTREX

PRIVATE AND CONFIDENTIAL

COMMENTS ON
FURTHER ELECTRICAL INDUCED POLARIZATION SURVEYS
OVER THE BOCO GRID, NEAR ROSEBERY, TASMANIA
ON BEHALF OF
ELECTROLYTIC ZINC COMPANY OF AUSTRALASIA LIMITED

BY

A.W. HOWLAND-ROSE
MSc,DIC,AMAusIMM,FGS
GEOPHYSICIST

SYDNEY, N.S.W.

MAY, 1978

TAS-051

002

255003

SCINTREX

CONTENTS

This Report is Appendix B of Report 78-1310

003

255004

SCINTREX PTY. LTD.

GEOPHYSICAL CONSULTANTS AND CONTRACTORS

SUMMARY

Further reconnaissance gradient array induced polarization surveys carried out in the Bulgobac area near Rosebery Tasmania have recorded some eleven zones of anomalous induced polarization which are characteristic of essentially disseminated chargeable material within resistive hosts. None are considered of primary interest.

Some five anomalies located on the original survey were investigated using a 50 metre dipole-dipole array. These revealed essentially similar anomalies of similar magnitude but less resolution than those originally located on the gradient survey.

1031 WELLINGTON STREET,
WEST PERTH, 6005
WESTERN AUSTRALIA

TELEPHONE: 321 6934
TELEX: 92353
TELEGRAMS: SCINTREX, PERTH

6 TRAMORE PLACE,
KILLARNEY HEIGHTS, 2087
N.S.W. AUSTRALIA.

TELEPHONE: 451 5367
TELEX: 26859
TELEGRAMS: SCINTREX, SYDNEY

SCINTREX

COMMENTS ON
FURTHER ELECTRICAL INDUCED POLARIZATION SURVEYS
OVER THE BOCO GRID, NEAR ROSEBERY, TASMANIA
ON BEHALF OF
ELECTROLYTIC ZINC COMPANY OF AUSTRALASIA LIMITED

INTRODUCTION

Following on gradient array electrical induced polarization surveys carried out over the Boco grid over three separate periods in April, May and July, 1976 and described in Scintrex report TAS-033 dated October/November, 1976, some 15½ kilometres of gradient array extensions to the area were surveyed on about 14 production days between 31st September and 14th October, 1977. In addition, some five dipole-dipole set-ups over anomalies located on the original gradient array surveys were read. These had to be repeated due to an instrument fault and this was done in February and April, 1978.

The gradient array survey was executed by R. Sims, while the repeat dipole-dipole surveys were undertaken by B. Ekstrom, R. Sims and R. Bennett.

The magnetic field data was surveyed and supplied by Electrolytic Zinc Company of Australasia Limited.

DATA PRESENTATION

The dipole-dipole data is presented on standard Scintrex dipole-dipole sheets at the scale of 1:2500.

The gradient array reconnaissance survey data is plotted on a horizontal scale of 1:5000, and vertical scales of 1 centimetre = 2 milliseconds for chargeability, and 10 centimetres = 1 log cycle for resistivity expressed in ohm-metres, while the magnetic field data is shown at the scale of 1 centimetre = 10 gamma.

The above data was contoured onto the standard 1:5000 scale EZ map sheets on which the original 1976 survey data was contoured. Some modifications to the original contour data was necessary due to resurveying of the original grid lines showing some errors.

DIPOLE-DIPOLE SURVEYS

The repeat surveys carried out in February and April, 1978 were executed using Scintrex IPR-8 receivers employing a three slice programme. The chargeability is presented in *millivolts/volt*, while the original survey data was in terms of *milliseconds*. The approximate relationship between the two is as follows:

1 millisecond (Ms) = 1.45 millivolts/volt (mV/V)

Each of the set-ups is individually described below. All were surveyed using 50 metre a spacings from n = 1 to n = 5/6

LINE 16440N (9100E - 9500E) ANOMALY XX

Gradient Array Data ..... The original gradient array induced polarization high of 10 milliseconds was located between 9325E and 9400E superimposed on a low 3 milliseconds background to the west and a higher (but still low) background of 5 milliseconds to the east. The zone occurred some 100 metres within a relatively high 3000 ohm-metres unit, with resistivities falling to 200 ohm-metres west of about 9200E. The priority was assessed to be a 'B' (TAS-033, 1976 page 22)). The maximum depth inferred from the gradient array data was about 50 metres.

Dipole-Dipole Data ..... The dipole-dipole data shows chargeability responses of 18.1 millivolts/volt (12.5 milliseconds) and 16.8 millivolts/volt (11.6 milliseconds) at n = 1 centred either side of 9350E. The source is *between* 9325E and 9375E and at a depth of less than the spacing, namely 50 metres. This is confirmed by the double peak on the larger n = 2 to 6 spacings.

The resistivity data shows the chargeable source to lie on or close to a marked change in resistivities from 150 ohm-metres($\pm$) in the west to 4000 to 5000 ohm-metres in the east.

LINE 13080N (9800E - 10200E) ANOMALY VIII

Gradient Array Data ..... The gradient array reconnaissance survey recorded a 4 millisecond anomaly coincident with a 50% fall in

apparent resistivity centred on line 13080N at 10125E. The *form* and amplitude suggested it to be of minor interest only. (Priority 'D' - TAS-033, 1976 page 14). The profile shape suggested a maximum depth to source of about 50 metres.

Dipole-Dipole Data ..... n = 1 values for chargeability of 11.6 millivolts/volt (8 milliseconds) and 12.1 millivolts/volt (8.2 milliseconds) were recorded at 10125E and 10175E compared with backgrounds to east and west of 8.6 millivolts/volt (5.9 milliseconds) and 9.7 millivolts/volt (6.7 milliseconds). Over this section the resistivity also shows a substantial fall of 40% to 50%. This confirms the gradient array reconnaissance anomaly VIII to be of minor interest only.

RAILWAY

A substantial negative induced polarization response over the railway line centred at and to the immediate east of 10,000E did not cause anomalous conditions on the dipole-dipole data.

ANOMALY XI

Gradient Array Data ..... On line 13080N at 9730E a small 5 to 6 milliseconds response was recorded coincident with an 80% fall in apparent resistivity to 3000 ohm-metres. The source was assessed to be shallow. The anomaly was assessed to be of Priority 'B' (TAS-033, 1976, page 16).

Dipole-Dipole Data ..... At about 9825E a better than twice background

18.1 millivolts/volt (12.4 milliseconds) response was recorded, which, on consideration of gradient "end effect" (see diagram 2a TAS-033), and the volume sampled with the dipole-dipole array, probably represent the same source. The dipole-dipole data suggests a narrow source as the anomalism does not extend through n = 2 and greater. The maximum depth to source is less than the a spacing, i.e. 50 metres.

LINE 13720N (9200E - 9600E) ANOMALY XIII

Gradient Array Data ..... A distinct 8 to 10 milliseconds response was recorded on a 10 to 12 milliseconds background coincident with a significant change in resistivity from 2000 ohm-metres at 9360E to 6000 ohm-metres at 9425E. The maximum depth was estimated to be 20 metres and the priority assessed as 'B'. (TAS-033, 1976, page 18).

Dipole-Dipole Data ..... This data shows a distinct "double peak" anomaly starting at n = 1 at 9325E of 22 millivolts/volt (15 milliseconds) to 9425E of 25 millivolts/volt (17 milliseconds). This indicates a shallow source, considerably less than the a spacing of 50 metres, and is centred at 9375E. The 45° double peak anomalies on n = 2 to 6 merely represent the "interference pattern" of the two dipoles as they cross the shallow source, and does not indicate depth extent information.

The resistivity data on the dipole-dipole data ranges from 500 ohm-metres to 3000 ohm-metres and does not show the contact anomaly

form that the gradient array shows. However, the n = 6 apparent resistivity data is very similar to the gradient array data in *form* and *magnitude*.

LINE 13720N (11000E - 11300E) ANOMALY III

Gradient Array Data ..... The gradient array data showed a significant 12 milliseconds above 4± milliseconds background between 11100E and 11300E (allowing for pegging error), on line 13720N. The resistivity remained a high 2000 to 3000 ohm-metres over this zone. The source was interpreted as disseminated chargeable material within a resistive bedrock, and the maximum depth assessed as 20 metres. The response was considered of Priority 'B'. (TAS-033, 1976, page 11).

Dipole-Dipole Data ..... The dipole-dipole data indicates a significant increase in chargeability from 5 ±2 millivolts/volt (3½ ±1½ milliseconds) to the west, to over 30 millivolts/volt (20 milliseconds) at 11225E, and 25 millivolts/volt (17 milliseconds) for 100 metres to the west. These values are accompanied by 2½ fold increases in resistivity from east to west. The interpretation is a disseminated chargeable zone within resistive rocks between 11200E and 11300E (+?) The maximum depth to the source of the chargeability response is less than the dipole (50 metres) used.

A sharp drop off in the gradient array resistivity at about 11390E is matched by a significant resistivity drop off at about 11350E of 600 ohm-metres as against 1000 ohm-metres to the west.

LINE 13880N (9950E - 10250E) ANOMALY XVI

Gradient Array Data ..... The response of 7 milliseconds against a low 5 milliseconds background centred at 10070E was assessed to be of Priority 'B'. (TAS-033, 1976, page 19). The increase in apparent resistivity from 2000 ohm-metres to 15,000 ohm-metres inferred an extremely resistive host to the chargeable material. The maximum depth to source was assessed as 20 metres.

Subsequent drilling showed deeper overburden and a steep sub-altered profile, while sulphides were intersected at about 10075E.

Dipole-Dipole Data ..... The dipole-dipole chargeability data shows increased chargeability of 10.2 millivolts/volt (7 milliseconds) at 10025E and 11.7 millivolts/volt (8 milliseconds) at 10125E, with a low of 7 millivolts/volt (5 milliseconds) between these points (at 10075E). This pattern is taken up over two adjacent spacings as a "double peak" anomaly originally centred at 10050E and 10150E on the n = 1 spacing, and on subsequent increasing n spacings. This is interpreted as a broad 50 metres wide chargeable zone which lies within 50 metres of the surface. (This is a very similar interpretation to the gradient array data).

One noticeable difference is the very low resistivities recorded of less than 100 to 400 ohm-metres over the chargeability anomaly centred at 10070E. The gradient data shows average resistivities of over 2000 ohm-metres. The explanation is that the dipole-dipole resistivity is characteristic of the *overburden* and is in fact

comparable to sounding SX#3 at 13880N/10040E (TAS-033, 1976, page 26), which shows resistivity within the overburden of 500 ohm-metres±. The high gradient data infers that the more substantial electrode spacings penetrate the bedrock more deeply, and is thus more representative of it. This is suggested by Edwards' paper (see Appendix). This does not, however, invalidate the dipole-dipole data, particularly the chargeability data. When energised, a source within the bedrock would preferentially decay *over* the source within the less resistive overburden, and thus be detectable. Only when the overburden resistivities become grossly inhomogeneous will masking occur. The dipole-dipole data does not demonstrate that effect over the zones surveyed.

CONCLUSIONS

1 - It is concluded that the dipole-dipole in general confirms the anomalies located during the gradient array reconnaissance survey.

2 - In the author's opinion the priorities placed on the original gradient data would not be changed by the dipole-dipole surveys subsequently run.

3 - In the author's opinion the resolution and the ability to isolate relatively anomalous chargeable zones was superior with the gradient array. A 25 or 20 metres dipole-dipole spacing would, however, have given equal resolution for the shallower sources located.

4 - The dipole-dipole data obtained was comparable to the gradient array data for chargeability and was subject to normal geometric distortion by the overburden for the resistivity data.

GRADIENT ARRAY SURVEY

METHOD

Salient points on the method, equipment and nature of the results were made in report TAS-033, 1976, pages 2 to 4 and 7 to 9.

DISCUSSION OF RESULTS

Each of the more substantial above-background induced polarization responses is discussed in detail below.

ZONE 'A' *Line 11640N at 9240E (Priority 'B')*

Line 11960N at 9200E (Priority 'D')

Line 12120N at 9210E & 9250E (Priority 'B')

On line 11640N the 8 milliseconds above background anomaly was centred at 9240E within a *local* reduction of 30% in the otherwise high 5000 to 6000 ohm-metres resistivities. The source is interpreted as disseminated chargeable material having a maximum depth of about 20 metres at 9240E.

On line 11960N the response was minor and still within highly resistive rocks, but on line 12120N two separate maxima of 8 to 9

milliseconds above the 8 milliseconds background were recorded centred at 9210E and 9250E where the maximum depth to source in each case is less than 40 metres. Each anomaly is associated with a local fall in apparent resistivity (of 45% and 30% respectively) to 1800 ohm-metres and 2400 ohm-metres. The source is disseminated sulphides (or graphite) within a host less resistive than the enclosing rocks.

SUMMARY ... This anomaly indicates a disseminated or weakly interconnected source within a host less resistive than the enclosing material. The host contains increased magnetite, but it is not the sole source. On lines 11640N and 12120N the anomaly is of Priority 'B' at best.

ZONE 'B' *Line 11640N at 9370E (Priority 'D')*
Line 11960N at 9300E (Priority 'D')
Line 12120N at 9325E (Priority 'B')

On lines 11640N and 11960N the response recorded was 4 to 5 milliseconds above background and the resistivity data showed it to be less resistive than the enclosing rocks. Only on line 12120N was the anomaly more substantial at 8 milliseconds above background. The maximum depth to source is about 20 metres.

SUMMARY ... The source is again considered to be a disseminated sulphide or graphite within a host less resistive than the enclosing rocks. The source is at best of Priority 'B' on line 12120N.

ZONE 'C' *Line 12280N(?) at 8530E & 8690E*

Line 12600N at 8590E & 8630E

Line 12760N(?) at 8520E & 8570E

Two significant maxima were located on line 12600N. The 9 and 11 milliseconds above background responses were centred at 8590E and 8630E where the maximum depth to source is estimated to be less than 40 metres. The resistivity observed is reduced over these maxima, to 1500 ohm-metres.

The two maxima *may* pass across line 12760N at 8520E and 8570E as very minor responses, and across line 12280N at 8530E and 8690E. However, only on line 12600N is the anomaly significant.

SUMMARY ... Significant maxima at 8590E and 8630E are interpreted as being due to disseminated sulphides (or graphite) within a less resistive host at a maximum depth of 40 metres.

ZONE 'DN' *Line 12760N at 8375E (Priority 'D/C')*

Line 12600N at 8430E (Priority 'B')

The anomaly is best displayed on line 12600N centred at 8430E, where a 10 milliseconds above 12 milliseconds background was recorded over material whose resistivity is about 1200 ohm-metres. Resistivities increase sharply to the east to reach 2000 ohm-metres at 8460E. The source is interpreted as disseminated or electrically discontinuous sulphides or graphite at a maximum depth of 50 metres. On line 12760N a minor 3 milliseconds anomaly at 8375E is associated with low 1100 ohm-metres resistivities which rise to 7500 ohm-metres

only 100 metres to the west. The maximum depth to source is interpreted as 50 metres.

SUMMARY ... The sources on both lines are interpreted to be disseminated sulphides or graphite within a host less resistive than the enclosing rocks. The maximum depth to source is about 50 metres. The anomaly is of Priority 'B' on line 12600N.

ZONE 'DS' *Line 11960N at 8475E*

Line 11640N at 8475E

Significant, if moderate, induced polarization responses of 6 to 8 milliseconds were recorded on the above lines, and in each case an apparent resistivity low was recorded some 10 metres to the east. The resistivities remain high, however, thus the source is interpreted as being due to disseminated chargeable material within a host less conductive than the enclosing rocks.

ZONE 'E' *Line 12920N at 8800E (Priority 'C/B')*

Line 12760N at 8850E (Priority 'C')

Line 12600N at 8900E (Priority 'D')

A *formational* type increase in chargeability was centred on lines 12600N to 12920N as set out above. As all lie within resistive 1500 to 3500 ohm-metres units, the source is considered to be disseminated sulphides within a resistive host. The response is best developed on line 12920N at 8800E where the source has a maximum depth of 50 metres.

SUMMARY ... The disseminated source is considered of formational origin.

ZONE 'F'	*Line 13720N*	*at*	*8370E*	*(Priority 'B+')*
	Line 13400N	*at*	*8340E*	*(Priority 'B')*
	Line 13240N	*at*	*8350E*	*(Priority 'C')*
	Line 13080N	*at*	*8340E*	*(Priority 'B/C')*

The anomaly is best developed on line 13720N where a 14 milliseconds, above the 10 milliseconds background, response was recorded. The anomaly on this line is broad and overall is associated with a fall in background resistivity to 600 ohm-metres. However, a sharp local rise was noted at 8370E. The maximum depth to source is estimated at 70 metres, and multiple sources are inferred at 8300E, 8370E and 8430E. On line 13400N the major source was 10 milliseconds above background at 8340E coincident with a discrete resistivity low of 500 ohm-metres as against the 1000 ohm-metres background. Multiple sources are again inferred either side of the peak, while the maximum depth to source is about 60 metres. 8 milliseconds above background chargeabilities on line 13240N at 8350E are accompanied by high 1100 to 1200 ohm-metres resistivities, while on line 13080N a single narrow peak at 8340E is accompanied by an *increase* in resistivity to 2000 ohm-metres. The depth to source on this line is 40 metres.

SUMMARY ... The source is considered to be weakly interconnected sulphides or graphite in the northern part of the zone and becoming increasingly resistive to the south. The anomaly is open to the north, and on line 13720N is of Priority 'B' plus.

ZONE 'G' *Line 13400N at 8190E (Priority 'B')*

Line 13240N at 8150E (Priority 'B/C')

Line 13080N at 8230E (Priority 'B/C')

This zone is seen as a material anomaly on lines 13400N, 13240N and 13080N. On the most northerly line a 12 milliseconds above background response was associated with *higher* background resistivities while on the southerly line, 8 milliseconds responses were recorded with a *depression* in apparent resistivity. The maximum depth to source is considered to be 65 metres, 50 metres and 50 metres respectively.

SUMMARY ... The source is considered to be disseminated chargeable material within a more resistive host on line 13400N, while to the south, less resistive rocks host the source.

ZONE 'H' *Line 13720N at 8730E (Priority 'C')*

Line 13400N at 8655E (Priority 'B')

Only on line 13400N is the anomaly significant. There, a 7 to 9 milliseconds above background response was recorded coincident with 700 ohm-metres resistivities as against 1300 to 2000 ohm-metres background. The maximum depth to source is calculated to be 50 metres.

SUMMARY ... A disseminated source within a less resistive host, or a weakly interconnected host, is the source. Of Priority 'B' on line 13400N and Priority 'C' on line 13720N.

ZONE 'I' *Line 13720N at 8600E (Priority 'C')*

This anomaly of 6 milliseconds above the 11 to 12 milliseconds background was recorded within a relatively low 1200 ohm-metres resistivity. The source is again considered to be disseminated. The maximum depth to source is 30 metres.

SUMMARY ... The disseminated source within a less resistive host is considered to be of Priority 'C')

ZONE 'J' *Line 14200N at 9010E*
Line 14040N at 9050E
Line 13880N at 8800E (Priority 'B')
Line 13720N at 8830E (Priority 'C')
Line 13400N at 8770E (Priority 'C')
Line 13240N at 8790E (Priority 'C')
Line 13080N at 8830E (Priority 'C')

This zone is a long "formational" type response which extends across the above lines.

On lines 13880N, 14040N and 14200N, the chargeability high is associated with a distinct resistivity low. The most significant responses were of 6 milliseconds at 8800E on line 13880N with a resistivity low of 1100 ohm-metres at 8830E, and on line 14200N where the chargeability is 6 milliseconds within a less resistive host. The maximum depth to source is about 30 to 45 metres on all lines, while the source itself is invariably disseminated.

SUMMARY ... The source is considered to be of formational origin and disseminated in nature. It may be a dextrally displaced extension of Zone 'E', which may itself be a dextrally displaced extension of Zones 'A/B'.

ZONE 'K' Line 14680N at 9055E (Priority 'C')

The most northerly anomaly located was situated at 9055E on line 14680N and is open to the north. The 1800 ohm-metres resistivities infer a generally resistive host to the source mineralisation. The magnetic field data shows a 25 gamma increase, inferring magnetite to be present within the source.

SUMMARY ... The sulphide (with magnetite) source is considered to be disseminated and contained within a resistive rock whose maximum depth is about 40 metres.

PHYSICAL PROPERTY CONTOUR INTERPRETATIONS

The three physical properties surveyed, namely, chargeability resistivity and total magnetic field, have been contoured onto the standard 1:5000 sheets. The best general fit has been attempted for each property. The three physical properties have been compiled into an interpretation plan which includes only the data from the present survey and compiled into a single sheet.

All three physical properties show a tendency to terminate along east-west to north-east/south-west trends. These trends have been termed "dislocations" on the interpretation plan. In the south,

these trends appear to show sinistral displacements in gross chargeability and total magnetic field. The apparent resistivity data also shows terminations against these trends, but the offsets along these trends are more difficult to ascertain. The dislocations may be due to faults, flexures or even facies changes, but they certainly represent major changes over which physical properties change.

The interpretation plan is a representation of the underlying physical properties and is thus a representation of the underlying geological units.

CONCLUSIONS

1 - The observed induced polarization background is, in common with the original survey, extremely low for the West Coast. This is due to an absence of chargeable material within the freshrocks.

2 - Each of the induced polarization anomalies located has been assigned a priority in the same manner as in the 1976 report (page 29, item 2). These are discussed in the main body of the report.

However, no anomalies akin to those observed over classical pyrite-lead-zinc mineralisation have been located on the present survey. Although the anomalism may well be due to pyrite-lead-zinc, this is not considered to be "massive" or substantial

across any of the lines surveyed in this case. This is not to say "end effects" have been observed on the lines covered, however, no truly "conductive" sources were inferred to exist across the lines surveyed.

4 - The contour interpretations of all three properties show a similar strike, while all show some degree of termination against grid east-west to north-east/south-west trending dislocations.

5 - As always, the relative merit of the geophysical anomalies located must be biased using available geological and geochemical data, and not primarily on *amplitude* or *form* of the anomalies defined by geophysical methods.

Respectfully submitted on behalf of:

SCINTREX PTY. LTD.

A.W. HOWLAND-ROSE, MSc,DIC,AMAusIMM,FGS.

GEOPHYSICIST

GEOPHYSICS, VOL. 41, NO. 6A (DECEMBER 1976), P. 1170-1183, 19 FIGS.

A FIELD TEST OF THE MAGNETOMETRIC RESISTIVITY (MMR) METHOD

R. N. EDWARDS* AND E. C. HOWELL‡

The electrical prospecting method, known as the Magnetometric Resistivity (MMR) method, is based on the measurement of the low level (about 100 milligamma), low-frequency (1–5 Hz) magnetic fields associated with noninductive current flow in the ground. The horizontal component of the magnetic field is measured along profiles which are at right angles to a baseline joining two widely separated current electrodes.

The field test was conducted on a plateau in the western cordillera, where the topography is characterized by steep hills, bold ridges, gullies and narrow canyons. A steep faulted contact between basement rocks of differing resistivity is exposed on one flank of the plateau, beneath over 500 m of Tertiary volcanics and sediments.

The object of the test was to determine if the basement contact could be mapped by the MMR method, working entirely on top of the plateau. The plan position of the contact could be inferred approximately from measurements at the outcrop.

The object was achieved with a minimum of data processing. Using a theoretical model which resembles a thick, outcropping vertical dike of infinite vertical extent, the contrast in resistivity across the contact is estimated. A further model, that of an exponential "alpha" center, is also fitted to the data in an effort to pin-point an anomalous region which may have unusually high conductivity.

INTRODUCTION

Electrical exploration methods have been used successfully for over half a century for locating base metal mineral deposits. They exploit the fact that these minerals are usually vastly better conductors of electricity than the basement rocks in which they occur. However, there are many areas of the world, of potential economic interest, where the basement is covered by overburden. The conductivity of the overburden is usually inhomogeneous, its average value being much larger than that of the basement rock. The overburden may often be associated with severe local topography, particularly if it is of recent volcanic origin.

Under these adverse conditions, many electrical methods become unreliable. The electromagnetic methods may not see through the overburden because electromagnetic disturbances cannot penetrate the conductive layer unless comparatively low frequencies are used. Even if data are obtained, as often as not their interpretation is very difficult, if it is possible at all.

The galvanic methods, such as resistivity, give very noisy data for two reasons. First, the electric field is being measured in a conductor. The acquisition of good data under these circumstances requires a prohibitively long integration time to improve the ratio of signal to instrumental noise. Second, superficial inhomogeneities in the conductivity of the overburden, or local topographic features, may distort the measured electric field and produce a form of noise which has a broad band of spatial wavelengths and which can effectively mask an anomaly due to a structure at depth. The presence of this noise is an inherent limitation of these methods.

This report describes the application of the Magnetometric Resistivity (MMR) method in a

Manuscript received by the Editor February 5, 1976; revised manuscript received April 1, 1976.
* University of Toronto, Toronto, Ont. M5S 1A7.
‡ Gulf Oil (Canada) Ltd., Calgary, Alta. T2P 2H7; formerly, University of Toronto.

region particularly difficult for prospection with conventional electrical methods. The overburden in the region is comparatively thick and is composed of about 300 m of Tertiary stream deposits, derived from older rocks, covered with about 300 m of Tertiary volcanics. The topography is characterized by steep hills, narrow canyons, gullies and bold ridges and it is typical of many prospects in the western cordillera.

The report should not be taken as a detailed case history but only as a field test of the magnetometric resistivity method itself. Its principal aim is to demonstrate that good data can be obtained in these regions and that they can be easily and successfully interpreted.

MAGNETOMETRIC RESISTIVITY (MMR) METHOD

The MMR method was first patented by Jakosky (1933) and a brief description of the method appears in his classic text on exploration geophysics (Jakosky, 1940). It is based on the measurement of the low level, low-frequency magnetic fields associated with noninductive current flow in the ground. The traditional resistivity method maps the electrical properties of the ground by measuring the electric field caused by galvanic current flow between a pair of current electrodes. The MMR method differs from it in that the potential electrodes are replaced by a sensitive coil or a magnetometer and a component of the magnetic field due to the current flow is recorded. The presence of an inhomogeneity redistributes the current flow which results in a perturbation of the electric field and, usually, of the magnetic field. The electric field immediately above a relatively conductive inhomogeneity must, by Ohm's law, be smaller than that expected for a uniform earth. The current density in this region is also reduced, but the current density within the inhomogeneity itself is enhanced so that the horizontal component of the magnetic field measured above the inhomogeneity is usually larger than that expected for a uniform earth.

There are many common configurations of the potential electrodes and the current electrodes in the resistivity method suitable for obtaining field measurements. Similarly, in the MMR method, one or both current electrodes may be moved with the magnetometer, either horizontally over the surface of the earth or vertically in a borehole. Alternatively, the current electrodes may be maintained in fixed positions and the magnetometer alone moved.

Perhaps the most useful MMR configuration is that which is comparable with the gradient array in resistivity. The horizontal component of the magnetic field at right angles to a line joining two widely spaced current electrodes is measured from place to place. Edwards (1974) recorded the first successful field survey using this array and also developed the methodology and the procedures for normalizing and interpreting the data which are used in this work. He points out that in the case of a two-dimensional structure, the current electrodes should be arranged to drive the current along the strike of the structure. The structure then looks like a set of resistors in parallel, which carry different currents, and a perturbation in the magnetic field must be produced. In contrast, for differences in the electric field to be produced, the current flow should be directed across the strike, so that the structure looks like a set of resistors in series, which have different potential differences across them.

Using a simple analog model, Edwards also demonstrates an important advantage of the MMR method over the resistivity method. The electric field can be severely distorted by local, insignificant inhomogeneities in conductivity or local fluctuations in topography whereas the magnetic field, being an integral over a volume distribution of current, is not greatly affected by the local distortion of current in a surface layer, provided that most of the current flow is not confined to the surface layer. It is this property of the method which prompted the work described here.

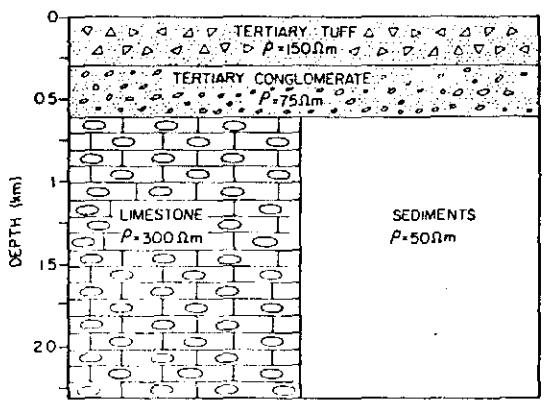

FIG. 1. The geologic section along the x axis of Figure 2. The resistivities shown are estimates based on measurements of the physical properties of drill cores.

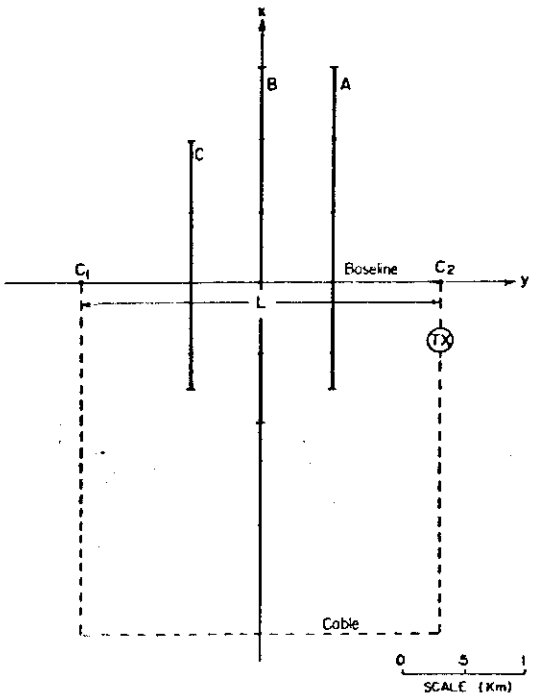

FIG. 2. A plan view of the experimental configuration. The ticks on lines A, B, and C are $.2L$ apart where L = 3048 m.

THE FIELD TEST

Introduction and objective

The field test was a joint project of the University of Toronto and Newmont Exploration Ltd. The test area is the top of a plateau believed to contain a steep, faulted contact, between basement rocks of moderate conductivity contrast, which lies beneath approximately 500 m of Tertiary volcanics and sediments. A simplified geological section is shown in Figure 1. The contact is exposed on one flank of the plateau, and its position under the test area may be inferred approximately from measurements at the outcrop. The test area has been previously utilized by Newmont Exploration Ltd. for various experimental purposes.

Locating the current electrodes

A plan view of the experimental configuration is shown in Figure 2. The current electrodes, C1 and C2, were located along and immediately above the expected strike of the structure, directing current flow parallel to the strike of the fault. A baseline, and y axis, is defined as the line joining C1 and C2. The point halfway between C1 and C2 is defined as the mid-point of the array. The principal profile of the array is also the x axis and it passes at right angles to the baseline through the mid-point of the array. The z axis is directed vertically downward.

In any MMR survey, the separation L of the current electrodes has to be determined theoretically before field work commences. In a uniform earth, the current flow will penetrate to a depth of the order of the electrode separation. However, if the overburden is more conductive than the basement rocks, then the current will tend to collect in the surface layer and not penetrate into the basement. Consequently, geologic structure in the basement may not be delineated.

In the Appendix, we derive a simple, useful function which may be used to determine approximately the percentage of current which remains in a thin conductive surface layer resting on a resistive half-space in terms of a dimensionless parameter α. The parameter $\alpha = 2S\rho/L$, where S is the conductivity-thickness product of the overburden and ρ is the resistivity of the basement. The function itself $f(\alpha)$ is given by

$$f(\alpha) = (100/\alpha)\{(\pi/2)[\mathbf{H}_1(1/\alpha) - Y_1(1/\alpha)] - 1\},$$

and it is plotted in Figure 3. The abbreviations $\mathbf{H}_1$ and Y_1 denote Struve's function and Bessel's function of the second kind, respectively, of order 1. The difference function $\mathbf{H}_1 - Y_1$ is tabulated by Abramowitz (1965). The percentage of the current which penetrates beneath the overburden is, of

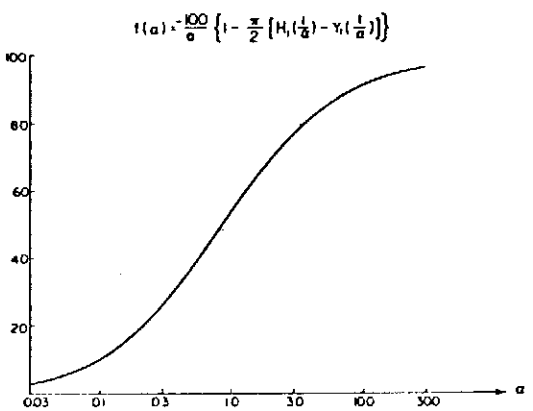

FIG. 3. The function $f(\alpha)$ which determines the percentage of current remaining in a conductive, thin surface layer above a resistive half-space.

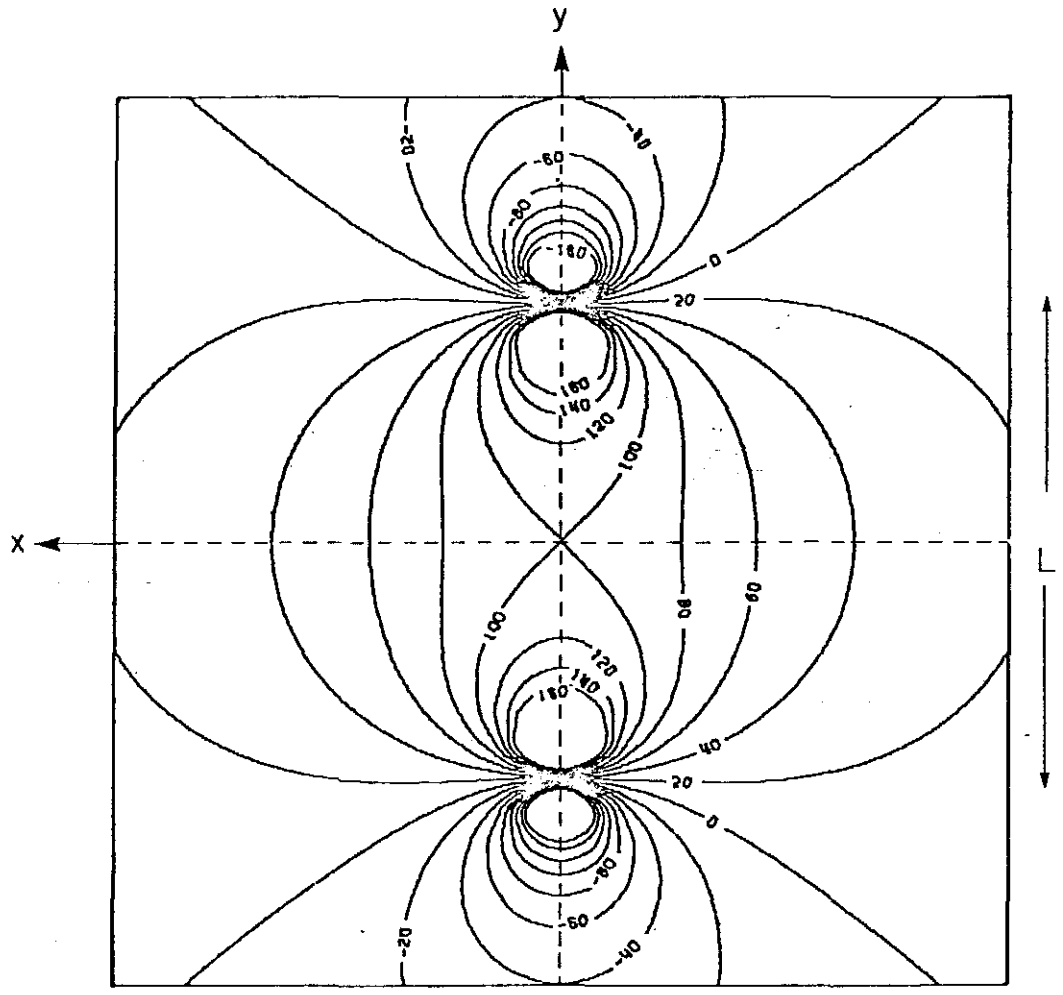

FIG. 4. The x-component of the normal magnetic field due to current flow between a pair of electrodes located on the y axis and separated by a distance L. The numbers on the contours are values of the component expressed as a percentage of the value at the center of the array. If L were 4000 m, the values would be in milligamma per ampère of current flow (after Edwards, 1974).

course, $100 - f(\alpha)$. By inspection of Figure 3, clearly L should be selected so that α is much less than 1.

A representative value of α for this survey is at most $1800/L$ where the overburden is assigned a conductivity-thickness product of 6 Se and the rocks beneath it a mean resistivity of 150 ohm-m. The selected value of L of 3048 m (10,000 ft) is a compromise. The corresponding value of α is 0.59 and consequently no less than about 70 percent of the transmitted current enters the basement rocks. A much larger value of L would reduce α but would not improve the delineation of the fault because its depth extent is limited.

Apparatus

A constant current of 2.5 A at a frequency of 3 Hz was generated by a Heinrichs-Geoex Mk 4b induced-polarization transmitter. A discussion of why this frequency is an optimum for the MMR method is given in Edwards (1974). Two no. 14 gauge copper wires connected the transmitter to the electrodes. These followed the three sides of the square outlined in Figure 2. The total resistance of the wire and the two current electrodes was about 120 ohm. In any MMR survey the wire loop has to be located carefully. If the loop is too close to a measurement site and if that site is

above or below the plane of the loop, then the current in the loop will produce a horizontal magnetic field at the site and contaminate the data. In this region of rough topography, the loop was placed as far as possible from a measurement site.

The magnetic field was measured using a Scintrex MFM3 high-sensitivity fluxgate magnetometer. This instrument is described by Seigel (1974) and its ability to recover sinusoidal signals of the order of 10 pT (10 milligamma) in amplitude over a time interval of about 30 sec was demonstrated by Edwards (1974). The output of the magnetometer is an analog voltage representing the measured magnetic field at 50 mV/nT. The magnetometer was connected directly into the input of a Heinrichs-Geoex Mk 4c induced-polarization receiver which measured the voltage and, hence, indirectly the magnetic field. About 5 minutes are required at each site to take a measurement.

Field observations and their reduction

Measurements of the x component of the magnetic field Bx were made at intervals of at most $.04L$ (122 m) along the three lines A, B, and C shown in Figure 2. All three lines are at right angles to the baseline. Line B coincides with the x axis, and lines A and C are at $y = .2L$ and $y = -.2L$, respectively.

The data were reduced in the following manner. First, the normal magnetic field Bx^n, expected over a uniform earth at each observation point, was calculated from the formula:

$$Bx^n(x, y) = (200I/L)\left[\frac{(2y/L) + 1}{(2x/L)^2 + ((2y/L) + 1)^2} - \frac{(2y/L) - 1}{(2x/L)^2 + ((2y/L) - 1)^2}\right],$$

which was derived by Edwards (1974). In common with all expressions for magnetic field given in this paper, the magnetic permeability is assumed to be that of free space, $4\pi \times 10^{-7}$ H/m, and I, L, and Bx^n are in amperes, meters, and nano-Tesla (gamma), respectively. The current is assumed to enter the ground at C2 and leave the ground at C1. The expression is plotted as a function of x and y in Figure 4, taken from Edwards (1974).

Second, the normal field is subtracted from the observed field $Bx(x, y)$, to give the anomalous field $Bx^a(x, y)$. Finally, the anomalous field is expressed as a percentage of the normal field value

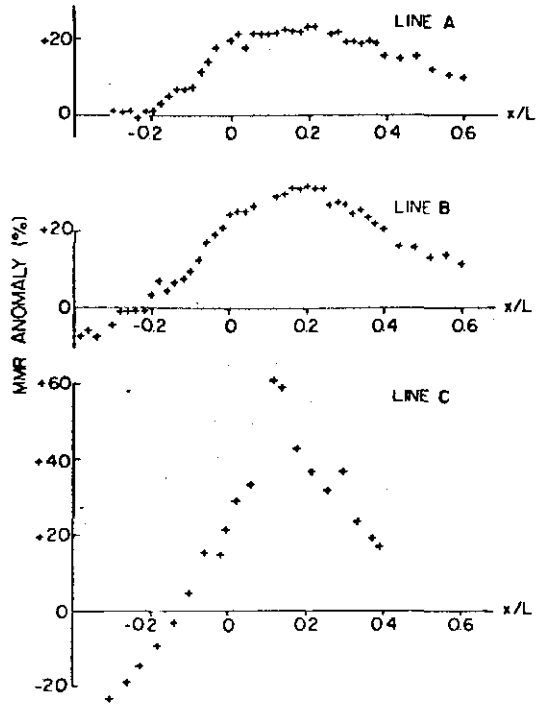

FIG. 5. The experimental MMR anomalies in the horizontal field measured along the lines A, B, and C shown in Figure 2.

at the center of the array $Bx^n(0, 0)$ where

$$Bx^n(0, 0) = 400I/L.$$

The result is defined as the dimensionless MMR anomaly in the horizontal field, i.e.,

$$\text{MMR anomaly} = 100(Bx(x, y) - Bx^n(x, y))/Bx^n(0, 0) = 100Bx^a(x, y)/Bx^n(0, 0).$$

The anomalies measured along lines A, B, and C are plotted as single profiles in Figure 5 and as a contour map in Figure 6. The errors in the observations are about 1 percent determined from the scatter of a few repeated observations. The short wavelength noise on the curves is not random. It is strongly correlated with the topography and is due in part to a horizontal field caused by current flow in the cables joining the electrodes to the transmitter and in part to the increased distance from the current flow in the ground. Both these effects have similar orders of magnitude and they have the same sign.

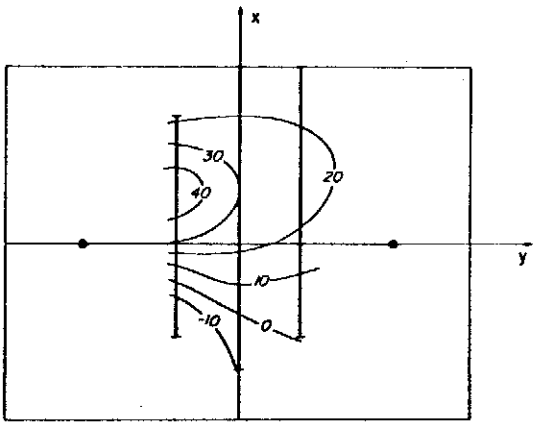

FIG. 6. A contour map of the MMR anomaly in the horizontal field. The contour interval is 10 percent.

INTERPRETATION OF THE DATA

Introduction

The data are interpreted using three models: a contact, an outcropping thick dike of infinite vertical extent, and a single exponential "alpha" center. The model of the contact was chosen because it is the simplest model that could possibly describe the geologic section of Figure 1. It proves to be a useful starting point enabling the strike of the expected structure to be located, mainly by studying the horizontal gradient of the MMR anomaly. The presence of a second contact is deduced.

The contact model leads naturally into the model of the thick dike. The two contacts delineated earlier can be simultaneously included in this model and a surprisingly good fit to the data is obtained. Estimates of the resistivity contrasts across the contacts are also determined. The model is limited in that it neglects the presence of the Tertiary overburden and also the limited depth extent of the contacts.

The overburden on its own produces no MMR anomaly, but it does elevate the plane of measurement to 500 m above the outcropping dike in the basement. This must have the effect of reducing the contributions to the observed anomaly of the larger wavenumbers, of the order of .002 m^{-1}. The anomaly is thus broader than the theoretical anomaly of an outcropping, thick dike. The extent of the broadening is under our investigation but is presently unknown. However, the effect may be difficult to observe on the profiles by eye as the greatest contributions to the anomaly come from wavenumbers of the order of .0003 m^{-1} ($1/L$), because the magnetic field is an integral over the whole current flow. Nevertheless, it should be possible to determine a "depth-to-target" from the profiles, provided the data are noise free over a wide band of wavenumbers. Depth-to-target information is perhaps better obtained using an alternative MMR method in which the current electrodes are expanded about a fixed central point where the magnetic field is measured.

The overburden also limits the amount of current that can be perturbed by the contacts. The estimates of the resistivity contrasts therefore are likely to be underestimates.

One feature of the data is poorly explained by the dike model; the increase in amplitude of the MMR anomaly from line A through line B to line C cannot be represented in a model of linear symmetry. A local conductive region or a change in geometry of the structure is required in the vicinity of $x = .15L$ on line C.

The exponential alpha center is an analytic approach to three-dimensional modeling. This type of model developed by Stefănescu (1950, 1970) and by Stefănescu and Stefănescu (1974) differs

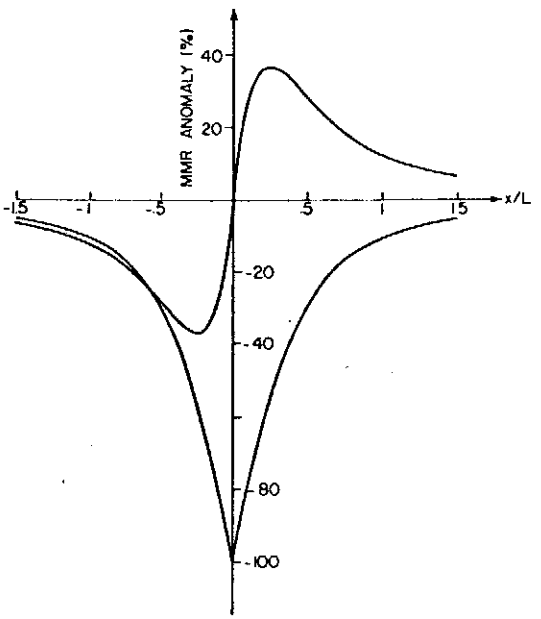

FIG. 7. The symmetric vertical MMR anomaly and the antisymmetric horizontal MMR anomaly due to two current electrodes embedded in a contact and separated by a distance L. The profiles are along the principal profile of the array.

from the better known models in that the boundaries between media are not sharply defined. Instead, the resistivity varies in a continuous fashion from point to point. The simulated model is that of a conductive center surrounded by a halo of resistive material whose conductivity decreases exponentially with distance from the center. This technique enables the region of higher conductivity to be pinpointed.

No doubt, the real structure is some combination of all these models and others. Clearly, the interpretation is limited. We are writing a numerical computer program to model a more realistic structure. Any conclusions drawn by the reader from the models should only be of a general nature.

The contact model

Referring to Figure 2, suppose that the quarter spaces in the ground defined by $(x < 0, z > 0)$ and $(x > 0, z > 0)$ have resistivities ρ_1 and ρ_2, respectively. Stefănescu and Nabighian (1962) show that the MMR anomaly in the horizontal field along the x axis, $100Bx^a(x, 0)/Bx^n(0, 0)$, is given by

$$(100k_{12}/\pi)\left[\frac{2x/L}{1+(2x/L)^2}\right]\log_e\left[\frac{1+(1/(1+(2x/L)^2)^{1/2})}{1-(1/(1+(2x/L)^2)^{1/2})}\right],$$

where $k_{12} = (\rho_1 - \rho_2)/(\rho_1 + \rho_2)$.

The corresponding anomaly in the vertical field, $100Bz^a(x, 0)/Bx^n(0, 0)$, is given by

$$-(100k_{12})\,[1 - (|2x/L|\,/(1+(2x/L)^2)^{1/2})].$$

The two expressions are plotted as a function of x/L in Figure 7, for the special case $k_{12} = 1$. The horizontal and vertical anomalies are, respectively, antisymmetric and symmetric about the contact. If the electrodes are not in the contact but some distance away from it, the anomalies maintain their symmetry about the contact, although their amplitudes reduce rapidly with increasing electrode offset. Therefore, an extremum in the vertical anomaly or in the horizontal gradient of the horizontal anomaly delineates the contact.

The horizontal gradient of the field data was determined for each of the profiles A, B, and C taken in turn. A fifth order polynomial in x was fitted by least-squares to the measurements on the profile. The analytic derivative of the polynomial was obtained and normalized such that its maximum value in the range $-.3L \le x \le .6L$ was unity. The resulting curves for the three profiles are presented in Figure 8. Two contacts are delineated, at about $x = -.15L$ and at about $x = .40L$, respectively. The former contact appears to be further from the baseline on line B than on either line A or line C.

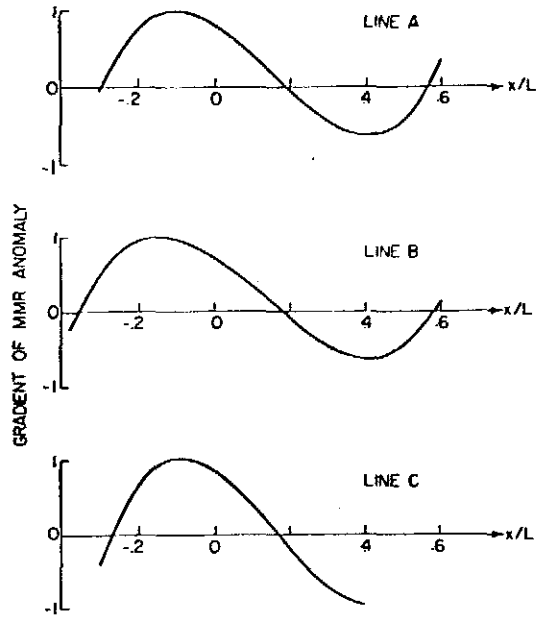

FIG. 8. The horizontal gradient of the MMR anomalies measured along the lines A, B, and C. The values on each line have been normalized independently to a maximum value of unity.

The thick, outcropping dike model

The second model, which includes three adjacent spaces 1, 2, and 3 of resistivities ρ_1, ρ_2, and ρ_3, respectively, looks like a thick, outcropping vertical dike of infinite vertical extent. The mathematical expressions describing the model, which follow, use a set of coordinates x, y, and z which differ slightly from those used previously. For convenience, the y axis does not pass through the electrodes but is moved temporarily so that the electrodes are located on the line $x = b$.

The plane $x = 0$ divides region 1 from region 2; the plane $x = d$, region 2 from region 3. Consider first, a single current electrode located at $(b, 0, 0)$ where a current I enters the ground. Edwards (1975), following exactly the method given by Stefănescu and Nabighian (1962), derives the anoma-

lous vertical magnetic field in regions 1, 2, and 3, Bz_1^a, Bz_2^a, and Bz_3^a as:

$$Bz_1^a = (100I/y)\left[k_{13} + (1 - k_{12})k_{32}\left\{\sum_{n=0}^{\infty}\frac{(k_{12}k_{32})^n(2(n+1)d - b - x)}{(y^2 + (2(n+1)d - b - x)^2)^{1/2}} + k_{12}\sum_{n=0}^{\infty}\frac{(k_{12}k_{32})^n(2(n+1)d + b - x)}{(y^2 + (2(n+1)d + b - x)^2)^{1/2}}\right\} - k_{12}\frac{(b-x)}{(y^2 + (b-x)^2)^{1/2}}\right],$$

$$Bz_2^a = (100I/y)\left[k_{13} + k_{32}\left\{\sum_{n=0}^{\infty}\frac{(k_{12}k_{32})^n(2(n+1)d - b - x)}{(y^2 + (2(n+1)d - b - x)^2)^{1/2}} + k_{12}\sum_{n=0}^{\infty}\frac{(k_{12}k_{32})^n(2(n+1)d + b - x)}{(y^2 + (2(n+1)d + b - x)^2)^{1/2}}\right\} - k_{12}\left\{\sum_{n=0}^{\infty}\frac{(k_{12}k_{32})^n(2nd + b + x)}{(y^2 + (2nd + b + x)^2)^{1/2}} + k_{32}\sum_{n=0}^{\infty}\frac{(k_{12}k_{32})^n(2(n+1)d - b + x)}{(y^2 + (2(n+1)d - b + x)^2)^{1/2}}\right\}\right],$$

and

$$Bz_3^a = (100I/y)\left[k_{13} - (1 - k_{32})k_{12}\left\{\sum_{n=0}^{\infty}\frac{(k_{12}k_{32})^n(2nd + b + x)}{(y^2 + (2nd + b + x)^2)^{1/2}} + k_{32}\sum_{n=0}^{\infty}\frac{(k_{12}k_{32})^n(2(n+1)d - b + x)}{(y^2 + (2(n+1)d - b + x)^2)^{1/2}}\right\} + k_{32}\frac{(x-b)}{(y^2 + (x-b)^2)^{1/2}}\right].$$

The reflection coefficients k_{ij} are given by $k_{ij} = (\rho_i - \rho_j)/(\rho_i + \rho_j)$.

The anomalous vertical field, due to two electrodes at $(b, -L/2, 0)$ and $(b, L/2, 0)$, is obtained by the superposition of solutions of the type given above for one electrode. The anomalous horizontal fields cannot be expressed so simply but may be derived from the vertical field through the surface convolution integrals of Skeels and Watson (1949) which are readily evaluated using Fourier transform techniques.

Using the starting values of $d = .55L$ and $b = .15L$, which are suggested from the preceding analysis of the gradient of the MMR anomaly, the parameters d, b, k_{12}, and k_{23} were altered until a best fit, in the least-squares sense, was obtained to the data on line B. Naturally, the computed horizontal fields have to be normalized in the same manner as the experimental data before any fit can be attempted. The values of the variables d, b, k_{12}, and k_{23}, corresponding to this best fit, were $.16L$, $.61L$, 5/7, and −9/11, respectively. In terms of the coordinates shown in Figure 2, this places the contacts at $x = -.16L$ and $x = .45L$, respectively.

The profiles computed for the three lines for this model are compared with the experimental profiles in Figure 9. Notice that the fit to line C is quite poor. It is impossible to fit the data on line C

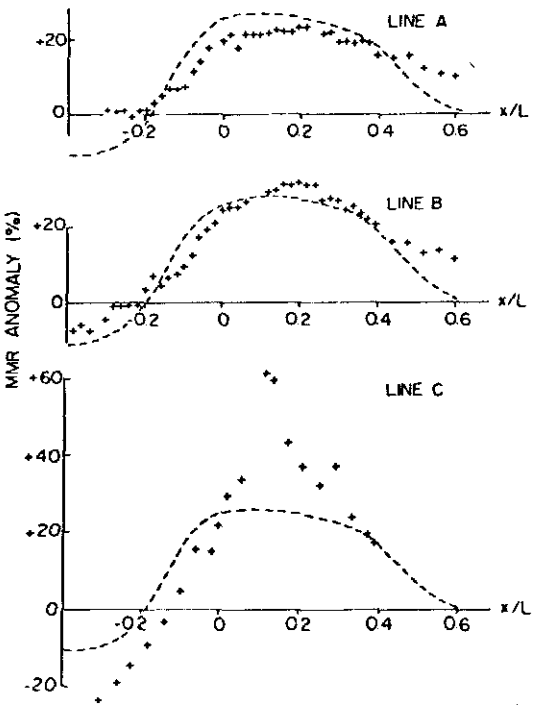

FIG. 9. The measured MMR anomalies along lines A, B, and C compared with the theoretical anomalies due to the best fitting dike model. The boundary between region 1 and region 2 is at $x = -.16L$, that between region 2 and region 3 is at $x = .45L$.

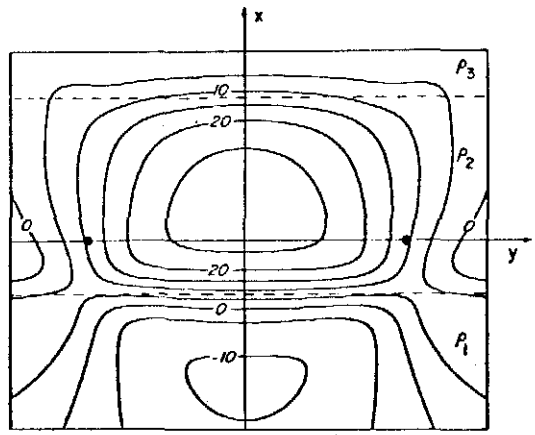

FIG. 10. A contour map of the theoretical MMR anomaly in the horizontal field due to the best fitting dike model (dashed lines). The electrodes are shown as black dots. The contour interval is 5 percent. The gradient of the field has extrema over the two contacts as shown by the bunching of the contours.

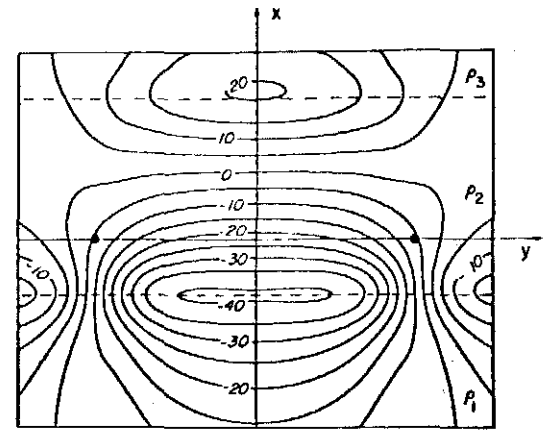

FIG. 11. A contour map of the theoretical MMR anomaly in the vertical field. The contour interval is 5 percent. The vertical field has extrema over the two contacts.

with this model, even if extreme values of the parameters are selected. The misfit is further demonstrated in Figure 10 which is a contour map of the theoretical anomaly. It should be compared with Figure 6.

For completeness, the corresponding vertical MMR anomaly is shown in Figure 11. It was from this map that the horizontal anomaly was calculated using the Skeels/Watson surface integrals.

The conductivity or alpha center model

The conductivity or alpha center model was introduced by Stefănescu (1950, 1970) in the following manner. The differential equation which relates the electric potential ϕ to the conductivity σ in a continuous, inhomogeneous medium is

$$\nabla\sigma \cdot \nabla\phi + \sigma\nabla^2\phi = 0.$$

The substitution

$$\alpha = \sqrt{\sigma} \text{ and } \psi = \alpha\phi$$

causes a separation of variables, and the equation reduces to two simultaneous equations

$$\nabla^2\alpha/\alpha = \nabla^2\psi/\psi = f,$$

where f is some function of position. If $f = k^2$, where k is a real positive constant, then the equations

$$\nabla^2\alpha - k^2\alpha = \nabla^2\psi - k^2\psi = 0$$

have two well-known elementary solutions with spherical symmetry, $\exp(\pm kR)/R$.

A general solution for α, consistent with the current boundary conditions at the earth's surface, the plane $z = 0$, is

$$\alpha = \sqrt{\alpha} = a_1[\exp(-kR)/R + \exp(-kR^*)/R^*] + a_2[\exp(+kR)/R + \exp(+kR^*)/R^*].$$

The variables R and R^* are defined in Figure 12. They represent the distances of a field point $M(x, y, z)$ from the alpha center $S(x_s, y_s, z_s)$ and the image of the center $S^*(x_s, y_s, -z_s)$ in the plane $z = 0$. The conductivity is a continuous function of position. It has axial symmetry about a vertical axis through S and S^* and a singular, maximum

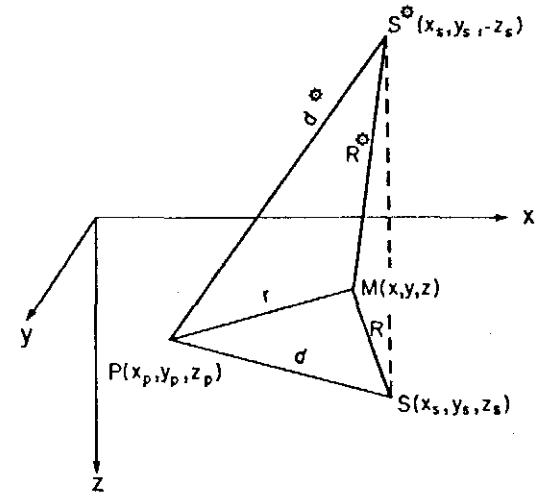

FIG. 12. The geometry of the alpha center. S is the center, S^* its image, M the field point, and P the current electrode.

value at S itself. Its variation elsewhere is determined by the parameters a_1, a_2, and k.

An analytic expression for the anomalous vertical magnetic field Bz^a, due to current flow from a single electrode $P(x_p, y_p, z_p)$ near an alpha center, was obtained by Tang Muoi (1972). It is

$$\begin{aligned} Bz^a(x, y, 0) = (400Iu/Ra)\,\{a_1(-\exp(-k(R+r))/r\,[1/(G_1G_2) + 1/(G_1^*G_2^*)] \\ + [\exp(-kd)/(dG_2G_3) + \exp(-kd^*)/(d^*G_2^*G_3^*)]) \\ + a_2(\exp(k(R-r))/r\,[1/(G_3G_4) + 1/(G_3^*G_4^*)] \\ - [\exp(-kd)/(dG_1G_4) + \exp(-kd^*)/(d^*G_1^*G_4^*)]) \\ - (R/r)\,[m/(dG_1G_3) + m^*/(d^*G_1^*G_3^*)]\}, \end{aligned}$$

where the variables $R = R^*$, d, d^*, and r are as shown in Figure 12, and

$$a = a_1[\exp(-kd)/d + \exp(-kd^*)/d^*] + a_2[\exp(+kd)/d + \exp(+kd^*)/d^*],$$

$$u = x(y_p - y_s) - y(x_p - x_s) + x_p y_s - x_s y_p,$$

$$m = a_1 \exp(-kd) + a_2 \exp(+kd),$$

$$m^* = a_1 \exp(-kd^*) + a_2 \exp(+kd^*),$$

$$G_1 = d + R + r,\ G_1^* = d^* + R + r,$$

$$G_2 = R + r - d,\ G_2^* = R + r - d^*,$$

$$G_3 = d - R + r,\ G_3^* = d^* - R + r,$$

$$G_4 = d + R - r,\ G_4^* = d^* + R - r.$$

Absolute values of resistivity cannot be determined by the MMR method. The anomalous magnetic fields for the dike and the contact depend on the reflection coefficients k_{ij}, or contrasts in resistivity. In the case of the alpha center, the field depends only upon the ratio of a_1 to a_2, so that a_1 and a_2 are not independent parameters. Nevertheless, a range of different models can be produced by varying a_1/a_2 and k.

Two typical models are illustrated in Figures 13 and 14. The parameters a_1/a_2 and k are, respectively, .01 and $.75/z_0$ and 100. and $.75/z_0$ for the two models. The values on the contours are of the logarithm, to base 10, of the resistivity, the zero contour being defined arbitrarily. If k is increased for a given a_1/a_2, then the contours bunch together around the alpha center and the overall geometry tends to look more like Figure 13 than Figure 14. Hence, when modeling, k and a_1/a_2 are often increased or decreased together.

Fitting an alpha center model to the observed MMR data is not a very straightforward process. There are essentially five variables, x_s, y_s, z_s, a_1/a_2,

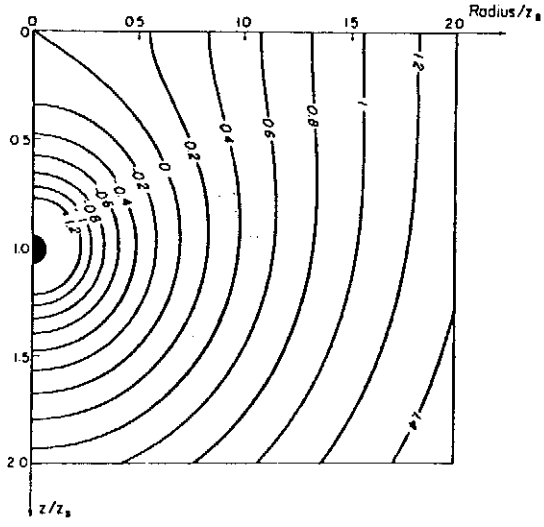

FIG. 13. The resistivity section about a typical alpha center. The parameters of the center are $a_1/a_2 = .01$, $k = .75/z_s$. The values on the contours are the logarithm of the resistivity to base 10. The zero contour was selected arbitrarily.

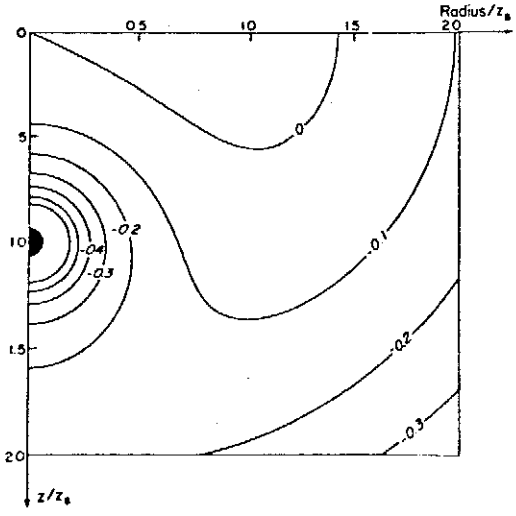

FIG. 14. The resistivity section of an alpha center whose parameters are $a_1/a_2 = 100$, $k = .75/z_s$.

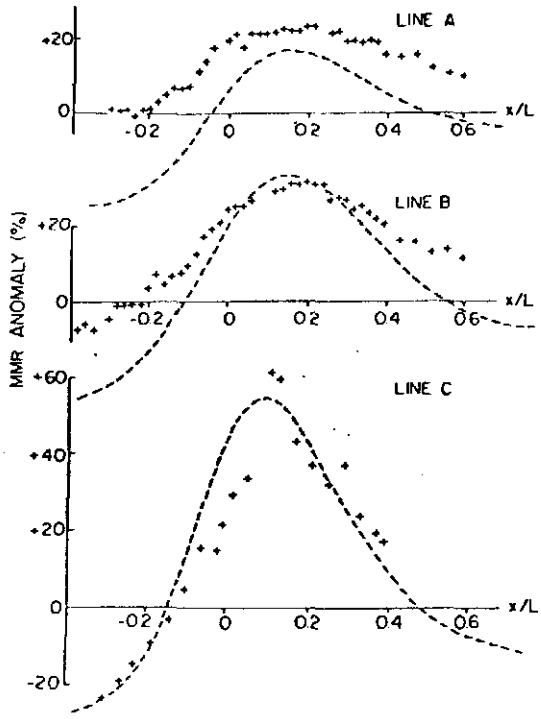

FIG. 15. The measured MMR anomalies along lines A, B, and C compared with the theoretical anomalies due to the alpha center model.

and k, all of which influence the horizontal field. As for the case of the dike, for every model the vertical field due to two electrodes in the vicinity of the center has to be computed and from it the horizontal field obtained through a numerical surface integral. Through experience and trial and error, the following very general properties of the model were determined.

Increasing the ratio a_1/a_2 increases the peak value of the horizontal field directly over the center. Increasing k decreases the half-width of a profile across the center. Increasing z_s both decreases the peak value and increases the half-width of the anomaly.

The guidelines used in the modeling were, first, to obtain a best fit to the data on line C and, second, to match the general features of the map of the data given in Figure 6. The values of the parameters in the final model were $x_s = .2L$, $y_s = -.14L$, $z_s = .58L$, $a_1/a_2 = 2.1 \times 10^4$, and $k = 6.08/L$. In Figure 15 the experimental data measured along the three lines are compared with those predicted by the model. The fit on line C is quite good, as one might expect, but the model does not match the data on the other two lines. However, the contour map of the model results given in Figure 16 matches tolerably the general features of Figure 6; for example, the elongated maximum directed toward the current electrode $C1$ is well represented. Again, for completeness, Figure 17 shows the vertical field anomaly corresponding to the horizontal anomaly of Figure 16.

A resistivity section through the selected alpha center is shown in Figure 18. How does one compare the resistivities in the real earth with those predicted by the model? Clearly, the resistivity of the real earth, in this area, does not change by so many orders of magnitude in such a short distance.

One scheme is to divide the section into three general zones: normal, conductive, and resistive. This division is not merely a function of the conductivity distribution but obviously has to depend upon where the current electrodes are located in relation to the distribution.

The resistive zone is perhaps the easiest to define. Current flow lines are essentially parallel to the resistivity contour which marks the edge of the zone, and little or no current flows within the zone. Any increase or decrease of resistivity within the zone should not be interpreted in terms of corresponding changes in the real earth.

Current flowlines cross the boundary of the conductive zone nearly at right angles. The zone appears to behave almost like a perfect conductor and, again, changes in resistivity within the zone are unlikely to be real.

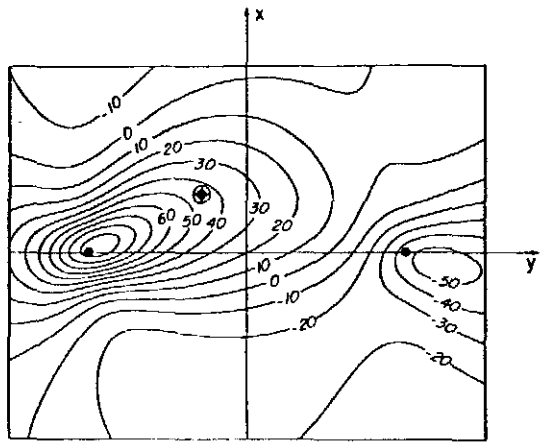

FIG. 16. A contour map of the theoretical MMR anomaly in the horizontal field due to the alpha center model. The contour interval is 10 percent. The horizontal anomaly is almost symmetric over the alpha epicenter, shown with a cross.

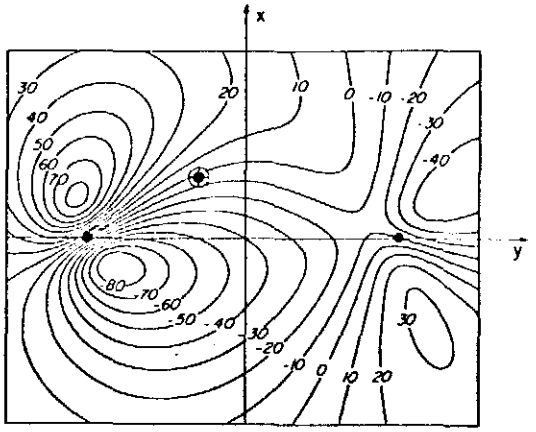

FIG. 17. A contour map of the theoretical MMR anomaly in the vertical field. The contour interval is 10 percent. The vertical anomaly is almost antisymmetric over the alpha epicenter.

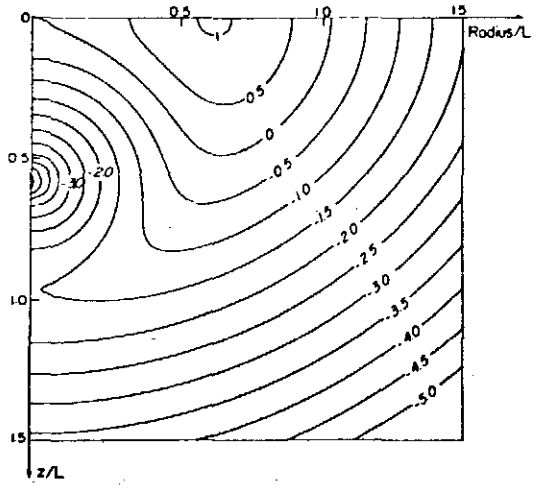

FIG. 18. The resistivity section of the alpha center model that was fitted to the data. The parameters are $a_1/a_2 = 2.1 \times 10^4$, $k = 6.08/L$, $z_a = .58L$.

The normal zone lies between the conductive zone and the resistive zone. Current flowlines cross resistivity contours in the normal zone at acute angles. Changes in resistivity within the zone should be identified with corresponding changes in the real earth.

Before the section of Figure 18 is qualitatively divided into zones, the relation of the current electrodes to the distribution should be noted. $C1$ and $C2$ are $.41L$ and $.67L$ from the alpha epicenter, respectively. Current flow from $C2$ to the alpha center is blocked by an annulus of resistive material. It seems reasonable to define the -1 contour as the boundary between a normal zone and a conductive zone. This definition appears to be consistent with the geology, placing the top of the conductor immediately above the alpha center at a depth of $.22L$ or 670 m.

In some respects, the alpha center model does not differ greatly in form from the dike model. It, too, in section has three spaces, a conductive space sandwiched between two resistive spaces. The conductive zone at large distances from the center should have no great effect on the overall current flow.

CONCLUDING REMARKS

The field test described in this paper does demonstrate that the MMR method works. The test was conducted in a region of severe topography where the overburden is quite thick, and where no other geophysical method has given equivalent data. The interpretation is consistent with the geology, and the object of the survey, delineation of a deep contact, was achieved with the minimum of data processing. Additional modeling of the data revealed a second contact and a local region of high conductivity was mapped. The models used were all analytic: A more flexible numerical model of the buried thick dike might have enabled a "depth-to-target" to be inferred directly from the profiles.

ACKNOWLEDGMENTS

The authors would like to thank M. J. Davidson and the staff of Newmont Exploration Ltd. very much for making this project possible. The project was suggested by A. A. Brant, whose continuing support of geophysics at the University of Toronto is greatly appreciated. Many hours of most fruitful discussion with M. N. Nabighian, currently visiting professor at the University, are gratefully acknowledged. M. Godlewski assisted with the collection of the data. E.C.H. was supported by a grant from the National Research Council of Canada.

REFERENCES

Abramowitz, M., 1965, Struve functions and related functions, *in* Handbook of mathematical functions with formulas, graphs and mathematical tables: A. Abramowitz and I. A. Stegun, editors, New York, Dover Publishing Co.

Edwards, R. N., 1974, The magnetometric resistivity method and its application to the mapping of a fault: Can. J. Earth. Sci., v. 11, p. 1136–1156.
———1975, The magnetometric resisitivity method: Paper presented at AIME annual meeting, New York, February 17, reprint no. 75-L-82.
Hurley, D. G., 1975, Boundary conditions for thin imperfect conductors and insulators: Geophys. Prosp., v. 23, p. 70–79.
Jakosky, J. J., 1933, Method and apparatus for determining underground structure: U. S. patent, no. 1906271.
———1940, Exploration geophysics: Los Angeles, Times-Mirror.
Seigel, H. O., 1974, The magnetic induced polarization (MIP) method: Geophysics, v. 39, p. 321–339.
Skeels, D. C., and Watson, R. J., 1949, Derivation of magnetic and gravitational quantities by surface integration: Geophysics, v. 14, p. 133–150.
Stefănescu, S. S., 1950, Modèles théoriques de milieux hétérogènes pour les méthodes de prospection électrique à courants stationnaires: Studii Technice şi Economice, ser. D, n. 2, p. 51–71, Bucurest.
——— 1970, Nouvelles applications de la théorie des milieux alpha harmoniques à la prospection electrique en courant continu: Geophys. Prosp., suppl. v. 28, p. 786–800.
Stefănescu, S. S., and Nabighian, M. N., 1962, Über magnetische störfelder als folge senkrechter schichtungen im gleichstrom: Rev. Géologie et Géographie, Acad. Repub. Pop. Roumaine, v. 6, p. 139–155.
Stefănescu, S. S., and Stefănescu, D., 1974, Mathematical models of conducting ore bodies for direct current electrical prospecting: Geophys. Prosp., v. 22, p. 246–261.
Tang, Muoi, 1972, Sur le champ magnetique des courants électriques stationaires dans les milieux hétérogènes alpha exponentiels: Rev. Roumaine de Géologie, Géophysique et Géographie, sér. Géophysique, v. 16, p. 51–90.

APPENDIX

Current flow from a point current pole in a thin conductive layer over a resistive half-space: Derivation of the function $f(\alpha)$.

A horizontal, thin conductive layer, of conductivity-thickness product S, is bounded by the planes $z = 0^-$ and $z = 0^+$ as shown in Figure 19. The half-spaces in the regions $z < 0^-$ and $z > 0^+$ have resistivities ρ_0 and ρ, respectively. A current pole, of strength I, is located at $z = -h$.

The electric potentials in the upper and lower regions may be written as

$$\phi_0(r, z) = (\rho_0 I/4\pi) \int_0^\infty (\exp(-u|z+h|) + A(u) \exp(uz)) J_0(ur)\, du,$$

and

$$\phi(r, z) = (\rho I/4\pi) \int_0^\infty (\exp(-u(z+h)) + B(u) \exp(-uz)) J_0(ur)\, du,$$

where r is the horizontal distance from the vertical axis through the current pole I.

The constants A and B are determined from the

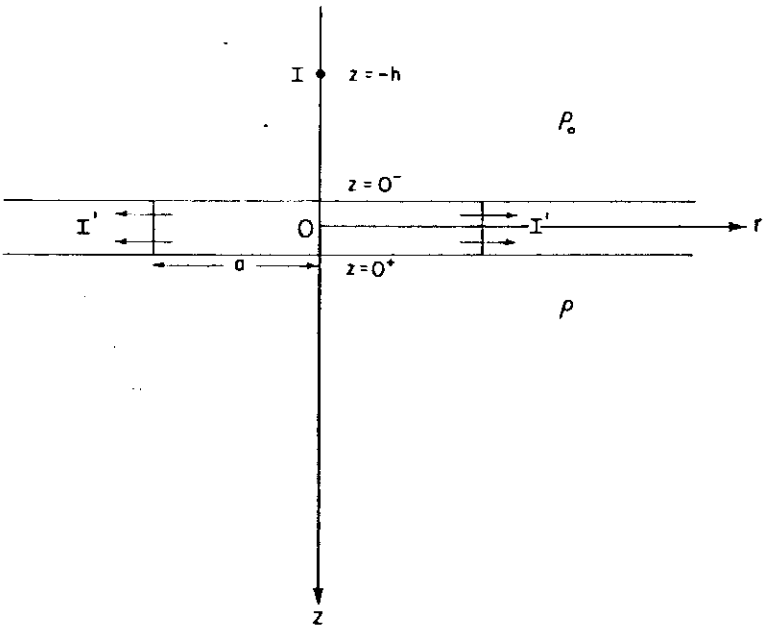

FIG. 19. The geometry of the thin conductive layer. In the practical case of a pole at the surface of the ground, $h = 0$ and $\rho_0 \gg \rho$.

two boundary conditions which define the thin conductive layer. First, there is no drop in potential across the layer, or

$$\phi_0|_{0^-} = \phi|_{0^+}.$$

Second, the differential form of the equation of continuity of current, applied to a small box in the layer, reduces to

$$(1/\rho_0)\left.\frac{\partial \phi_0}{\partial z}\right|_{0^-} = (1/\rho)\left.\frac{\partial \phi}{\partial z}\right|_{0^+} - S\left.\frac{\partial^2 \phi}{\partial z^2}\right|_{0^+}.$$

(A rigorous proof of this boundary condition has recently been given by Hurley, 1975.)

Solving these equations gives

$$A = (k - Ru)\exp(-uh)/(1 + Ru),$$

and

$$B = (-k - Ru)\exp(-uh)/(1 + Ru),$$

where

$$R = S\rho\rho_0/(\rho + \rho_0),$$

and

$$k = (\rho - \rho_0)/(\rho + \rho_0).$$

The tangential component of the electric field is continuous across a conductive layer. Hence, *within the layer*,

$$Er(r) = -\left.\frac{\partial \phi}{\partial r}\right|_{0^+}.$$

The practical case corresponds to a current pole at the surface of the ground, so that we set $h = 0$ and $\rho_0 \gg \rho$. Then,

$$Er(r) = (\rho I/2\pi)\int_0^\infty (u/(1 + S\rho u))J_1(ru)\,du.$$

The total current I' crossing the vertical edge of a thin horizontal disk, of radius a, in the layer is given by

$$\begin{aligned} I' &= 2\pi a S Er(a) \\ &= I\int_0^\infty (\alpha t/(1 + \alpha t))J_1(t)\,dt \\ &= I f(\alpha)/100, \end{aligned}$$

where the function $f(\alpha)$ represents the percentage of current which remains in the conductive layer at a distance a from the current pole, and the dimensionless parameter α is given by

$$\alpha = S\rho/a.$$

But,

$$1/(1 + \alpha t) = (1/\alpha)\int_0^\infty \exp(-ts)\exp(-s/\alpha)\,ds.$$

Hence,

$$f(\alpha) = 100\int_0^\infty \exp(-s/\alpha)\int_0^\infty \exp(-ts)tJ_1(t)\,dt\,ds.$$

Abramowitz (1965) lists a standard integral involving the Struve function H_0 and a Bessel function of the second kind Y_0, of the form

$$\begin{aligned} &(\pi/2)(\mathrm{H}_0(pq) - Y_0(pq)) \\ &= \int_0^\infty \exp(-ps)/(s^2 + q^2)^{1/2}\,ds \\ &= \int_0^\infty \exp(-ps)\int_0^\infty \exp(-ts)J_0(qt)\,dt\,ds. \end{aligned}$$

Differentiating both sides with respect to q yields

$$\begin{aligned} &(\pi p/2)[(2/\pi) - \mathrm{H}_1(pq) + Y_1(pq)] \\ &= -\int_0^\infty \exp(-ps)\int_0^\infty \exp(-ts)tJ_1(qt)\,dt\,ds. \end{aligned}$$

Hence, by inspection,

$$f(\alpha) = (100/\alpha)((\pi/2)(\mathrm{H}_1(1/\alpha) - Y_1(1/\alpha)) - 1).$$

036

255037

SCINTREX PTY. LTD.

INDUCED POLARIZATION AND RESISTIVITY SURVEY

DIPOLE - DIPOLE ARRAY

DATE 6 APRIL 1978

PLOTTED BY DICK SIMS

PULSE 2 SEC | Rx. 304126

DIPOLE SPACING 50m

LINE No. 16440 N (ZONE XX)

PROSPECT BULGOBAC BOCO GRID

JOB No. TAS-051 (RPT.)

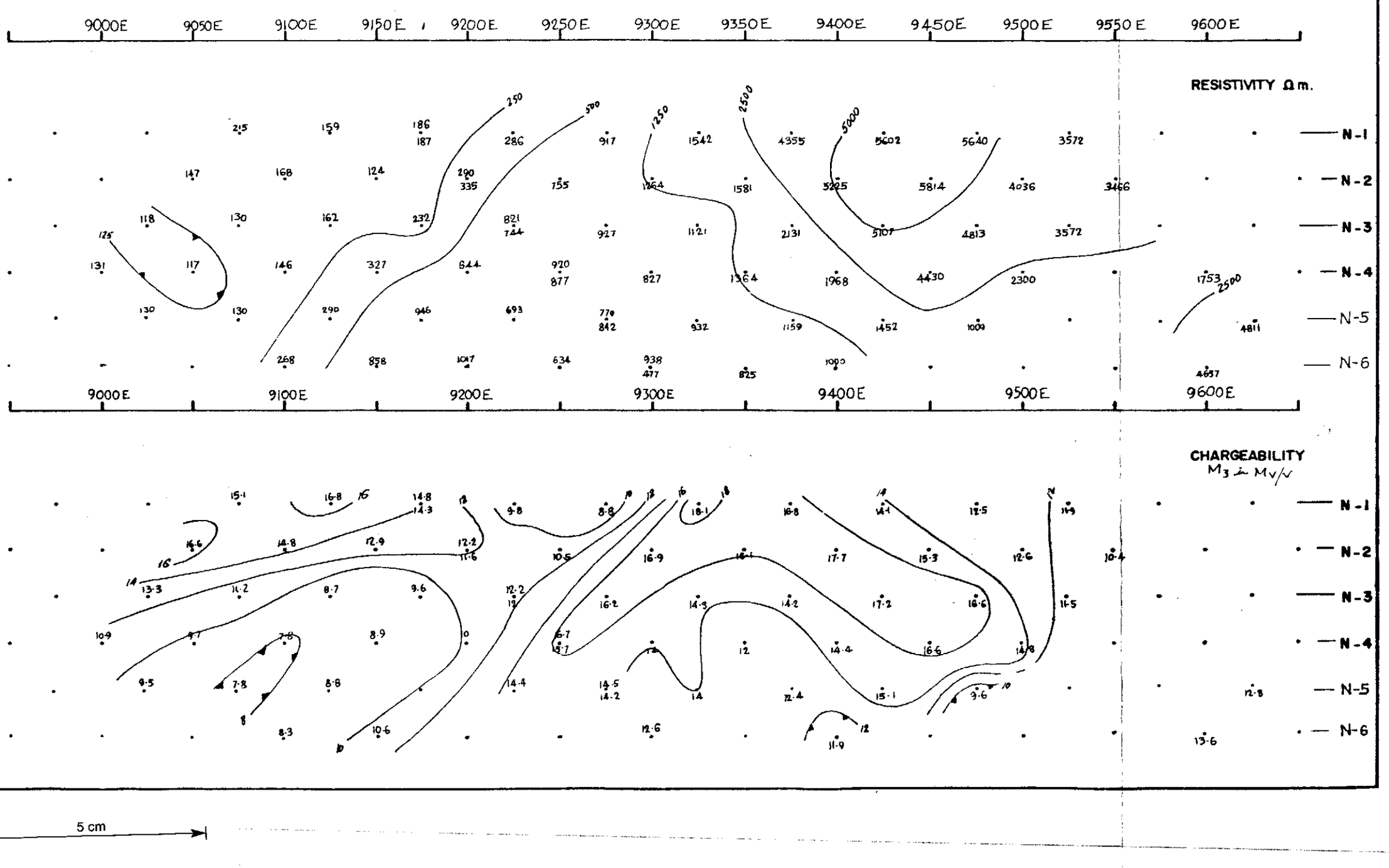

037

255038

SCINTREX PTY. LTD.

INDUCED POLARIZATION AND RESISTIVITY SURVEY

DIPOLE - DIPOLE ARRAY

DATE 7 APRIL 1978

PLOTTED BY DICK SIMS

PULSE 2 SEC | Rx. 304126

DIPOLE SPACING 50 M

LINE No. 13080 N ZONES VIII & XI

PROSPECT BULGOBAC BOCO GRID

JOB No. TAS-051 (RPT.)

9700E 9800E 9900E 10000E 10100E 10200E 10300E

Road Rail line River

RESISTIVITY Ω m.

N-1 N-2 N-3 N-4 N-5 N-6

CHARGEABILITY

M3 in Mv/v

N-1 N-2 N-3 N-4 N-5 N-6

5 cm

255039

033

SCINTREX PTY. LTD.

INDUCED POLARIZATION AND RESISTIVITY SURVEY

DIPOLE - DIPOLE ARRAY

DATE 4 APRIL 1978	
PLOTTED BY DICK SIMS	
PULSE 2 SEC	Rx. 304126
DIPOLE SPACING 50 M	

LINE No. 13720 N ZONE XIII

PROSPECT BULGOBAC BOCO GRID

JOB No. TAS-051 (RPT.)

9050E 9100E 9150E 9200E 9250E 9300E 9350E 9400E 9450E 9500E 9550E 9600E 9650E 9700E 9750E

RESISTIVITY Ω m.

N-1 N-2 N-3 N-4 N-5 N-6

CHARGEABILITY

M3 in Mv/v

N-1 N-2 N-3 N-4 N-5 N-6

5 cm

255040

039

SCINTREX PTY. LTD.

INDUCED POLARIZATION AND RESISTIVITY SURVEY

DIPOLE - DIPOLE ARRAY

DATE 18 FEB 1978

PLOTTED BY A.H-R.

PULSE 2 SEC | Rx. 304127

DIPOLE SPACING 50 M

LINE No. 13720N ZONE III

PROSPECT BULGOBAC BOCO-GRID

JOB No. TAS-051 (RPT.)

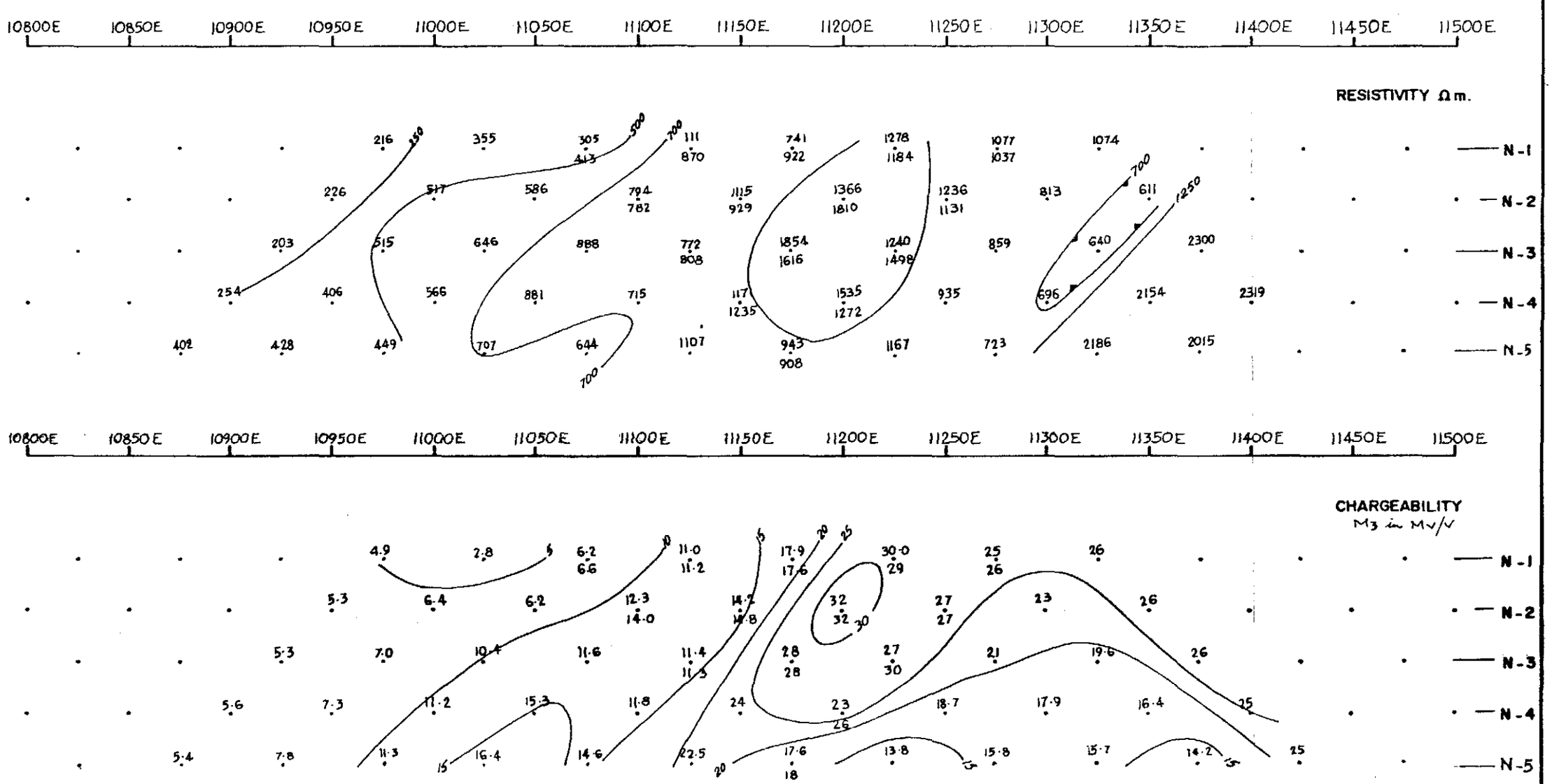

5 cm

255041

040

SCINTREX PTY. LTD.

INDUCED POLARIZATION AND RESISTIVITY SURVEY

DIPOLE - DIPOLE ARRAY

DATE 17 FEB 1978

PLOTTED BY A.H-R.

PULSE 2 SEC. | Rx. 340127

DIPOLE SPACING 50 M

LINE No. 13880 N ZONE XVI

PROSPECT BULGOBAC
BOCO-GRID

JOB No. TAS-051 (RPT)

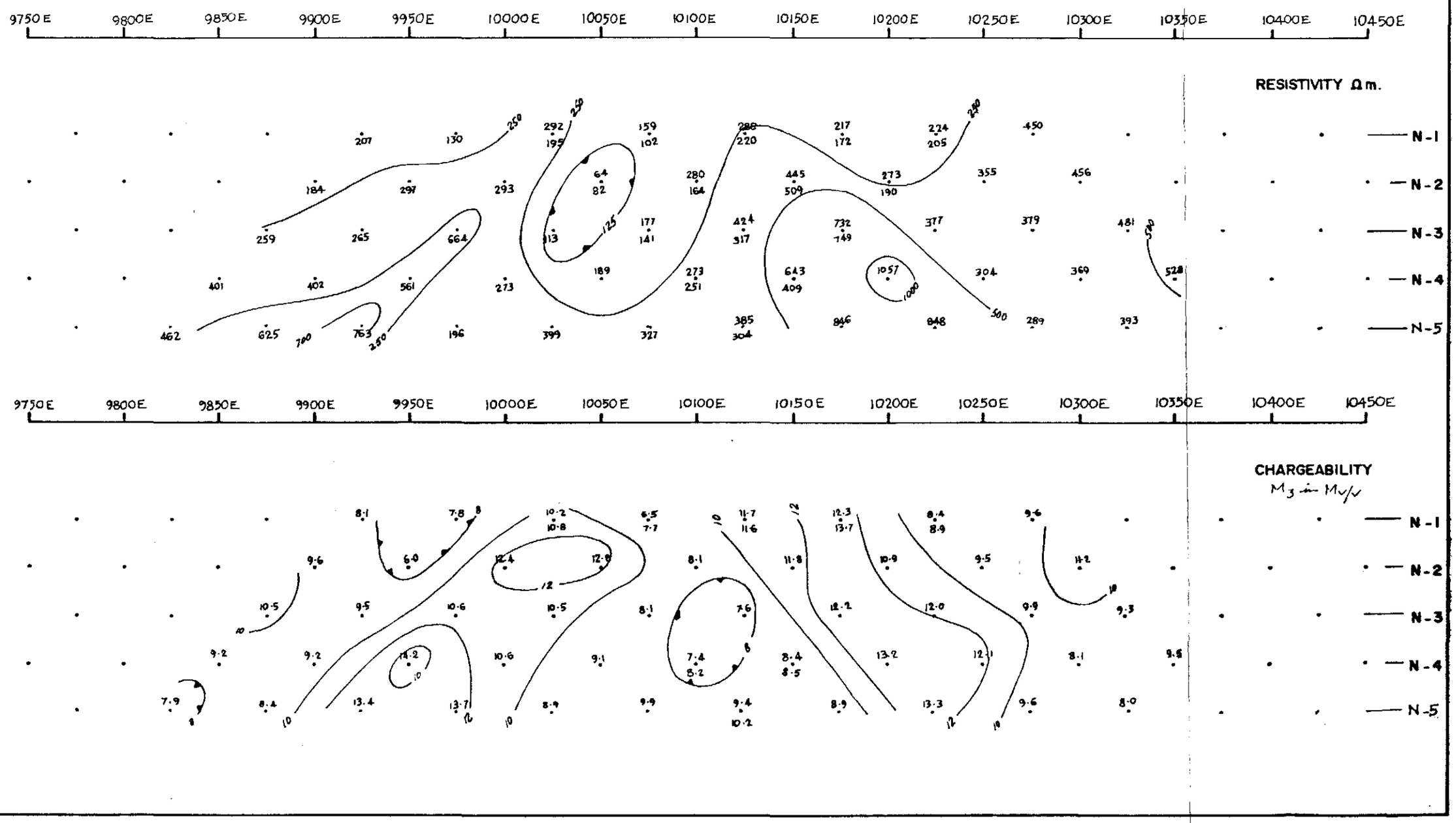

5 cm

041

255042

LINE 14880N

Bulgobac - Boco Grid

Gradient Array EIP

TAS-051

62,700
δ

62,650
δ

62,600
δ

ρ_a
Ω-M
5,000
2,000
1,000

M
ms
20
16
12
8
4
0

RAILWAY LINE & WATER CATCHMENT

NE

ρ_a

9100E
9300E
9500E

5 cm

042

255043

LINE 14680 N

Bulgobac - Boco Grid

Gradient Array EIP

TAS -051

62,700 γ

62,650 γ

62,600 γ

M mS

24

20

16

12

8

4

0

ρ_a ΩM

5,000

2,000

1,000

K

M

ρ_a

8900E

9100E

9300E

9500E

5 cm

255044

045

LINE 14520 N

Bulgobac - Boco Grid

Gradient Array E.I.P

TAS-051

62,700 f
γ

62,650 f
γ

ρ_a M
5,000

M
ms
20
16
12
8
4
0

62,600 f
γ

2,000

1,000

noise

ρ_a

M

8300E

8500E

8700E

8900E

9100E

9300E

9500E

5 cm

255045

LINE 14360 N

Bulgobac - Boco Grid

Gradient Array E.I.P.

TAS -051

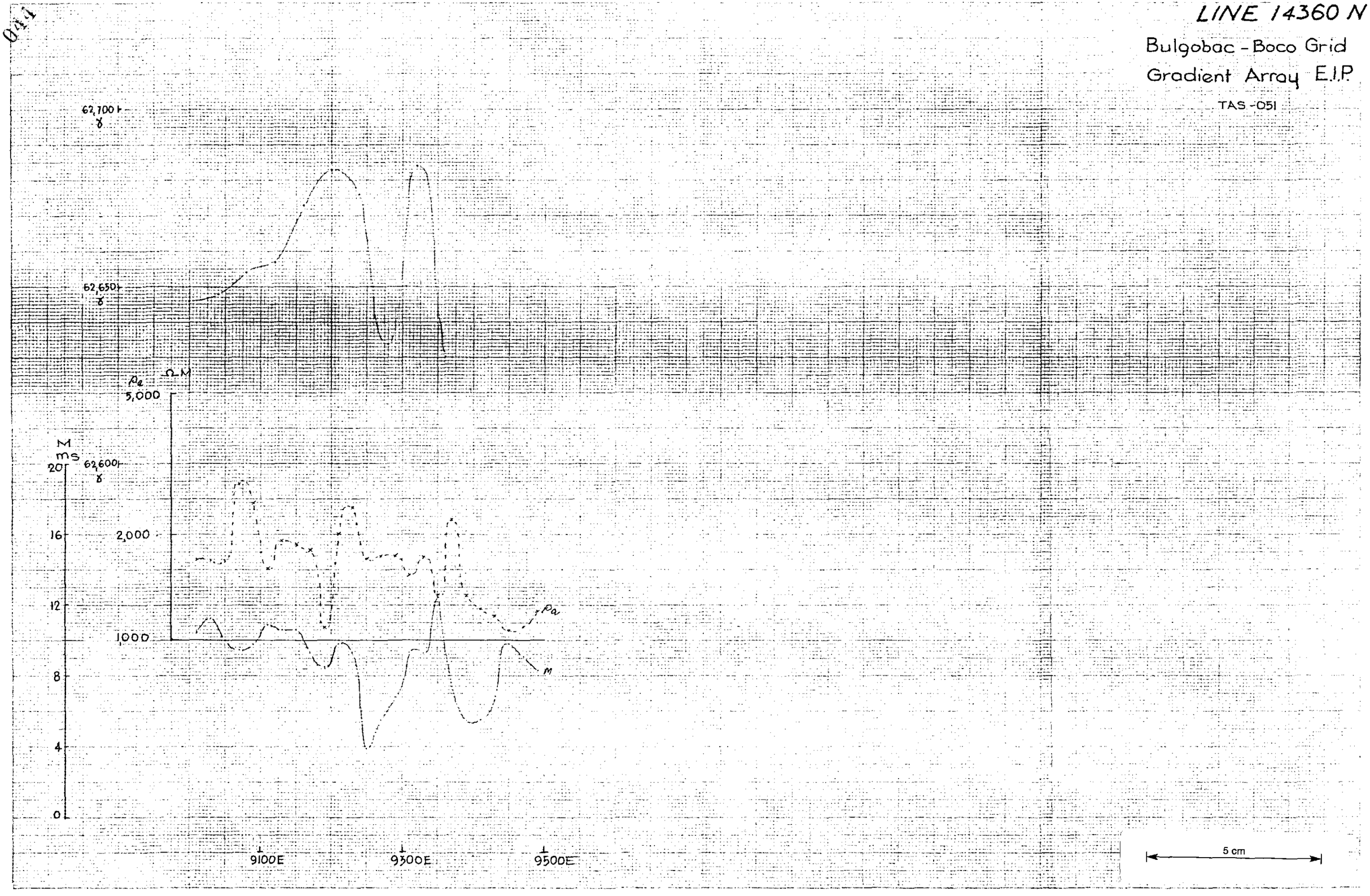

045

255046

LINE 14200 N

Bulgobac - Boco Grid

Gradient Array E.I.P

TAS - 051

62,700γ

62,650γ

62,600γ

ρ_a Ω-M

10,000

5,000

2,000

1,000

5,000

J^N

ρ_a

M

24

20

16

12

8

4

0

8500E

8700E

8900E

9100E

9300E

9500E

5 cm

046

255047

LINE 14040 N

Bulgobac - Boco Grid
Gradient Array E.I.P.

TAS - 051

62,700 γ

62,650 γ

62,600 γ

ρ_a Ω M

10,000

5,000

2,000

1,000

M mS

24

20

16

12

8

4

0

ρ_a

J

M

8900E

9100E

9300E

9500E

5 cm

255048

LINE 13880 N

Bulgobac - Boco Grid

Gradient Array E.I.P.

TAS-051

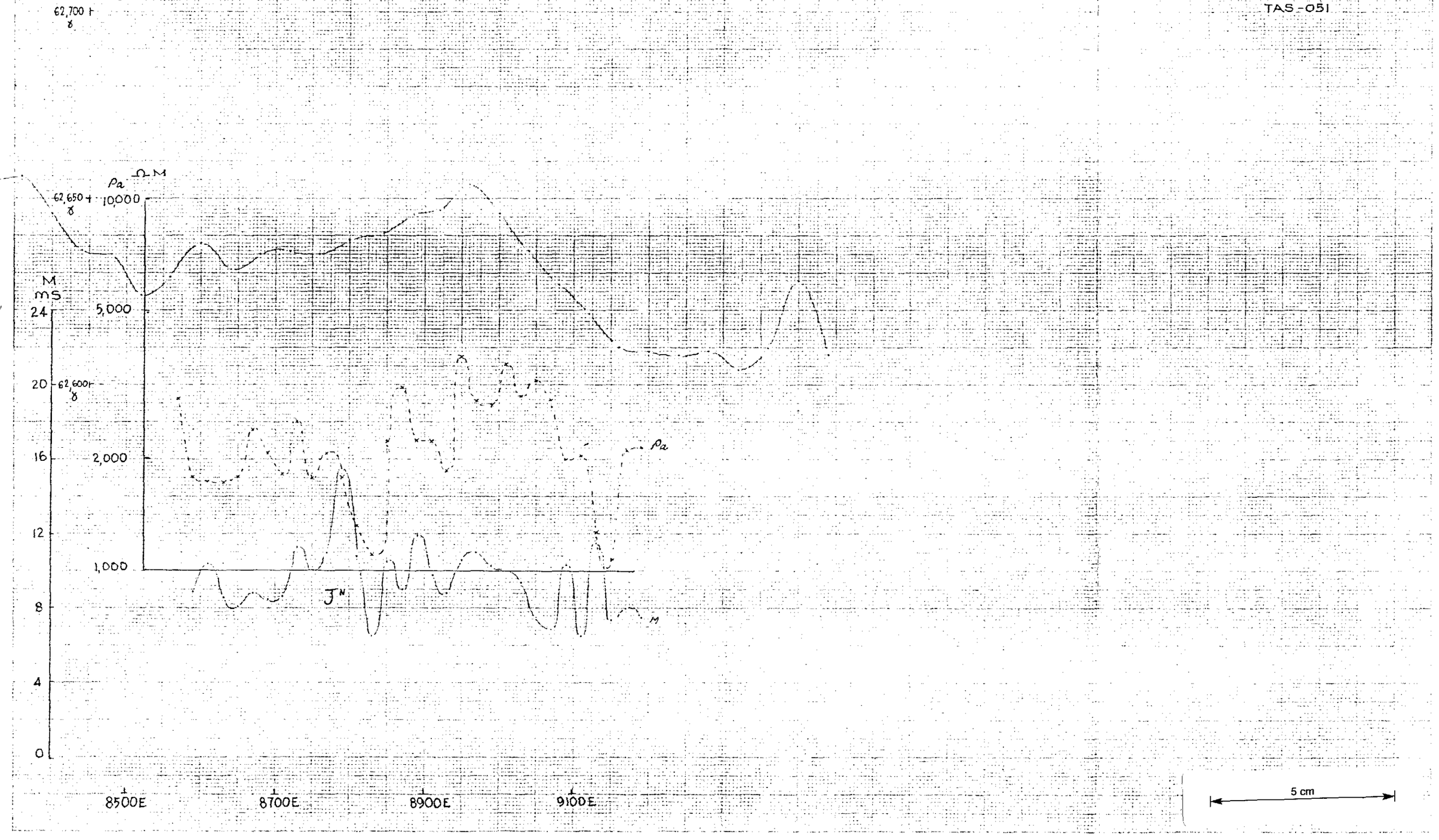

043

255045

LINE 13720 N

Bulgobac - Boco Grid

Gradient Array EIP

TAS-051

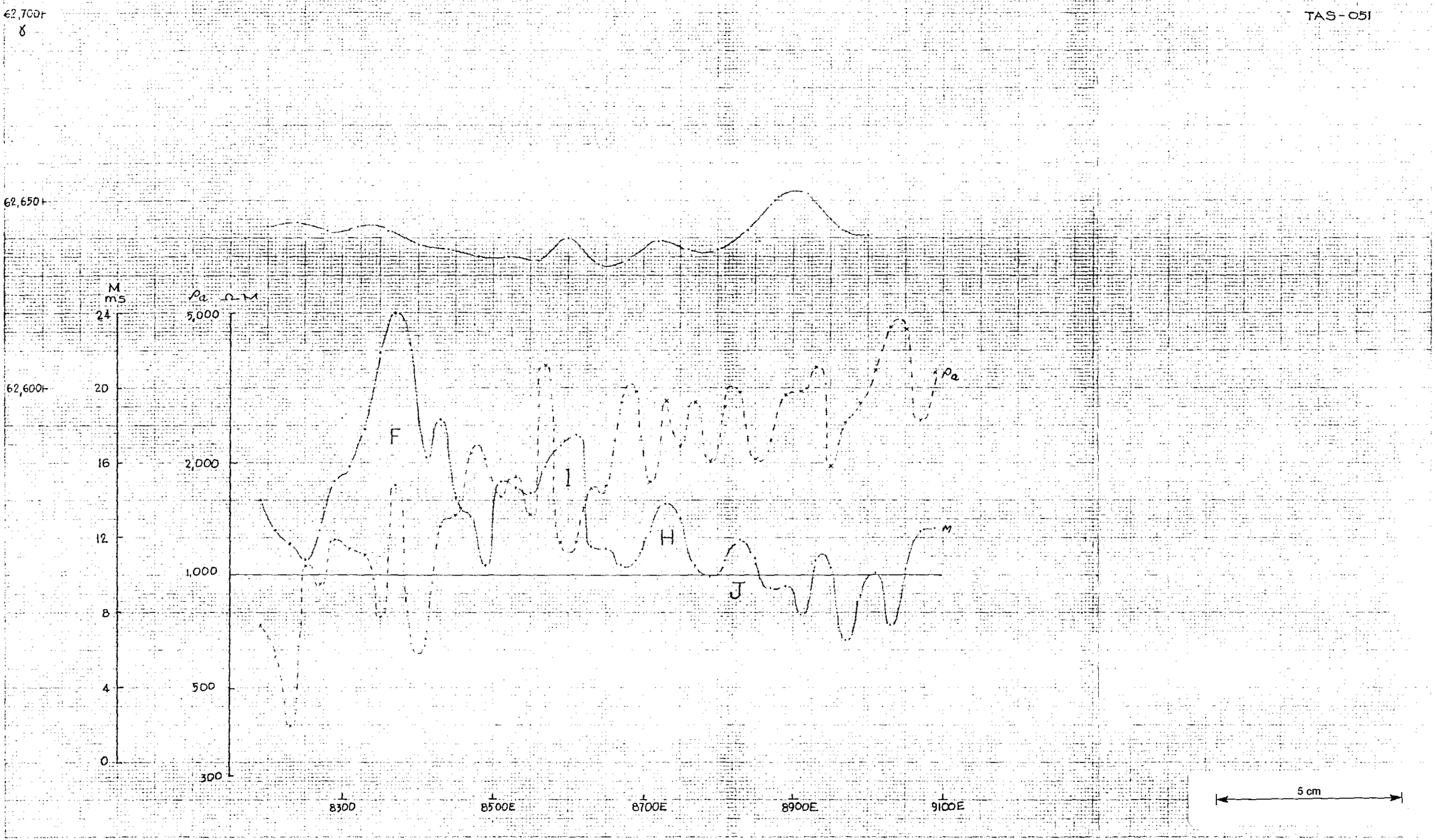

049

255050

LINE 13400 N

Bulgobac - Boco grid

Gradient Array EIP

TAS-051

62,700 γ

62,650 γ

62,600 γ

M ms

Ωm Ρa 5,000

2,000

1,000

24

20

16

12

8

4

0

G

F

H

Js

M

Ρa

8100E

8300E

8500E

8700E

8900E

9100E

5 cm

050

255051

LINE 13240 N

Bulgobac - Boco Grid

Gradient Array EIP

TAS - 051

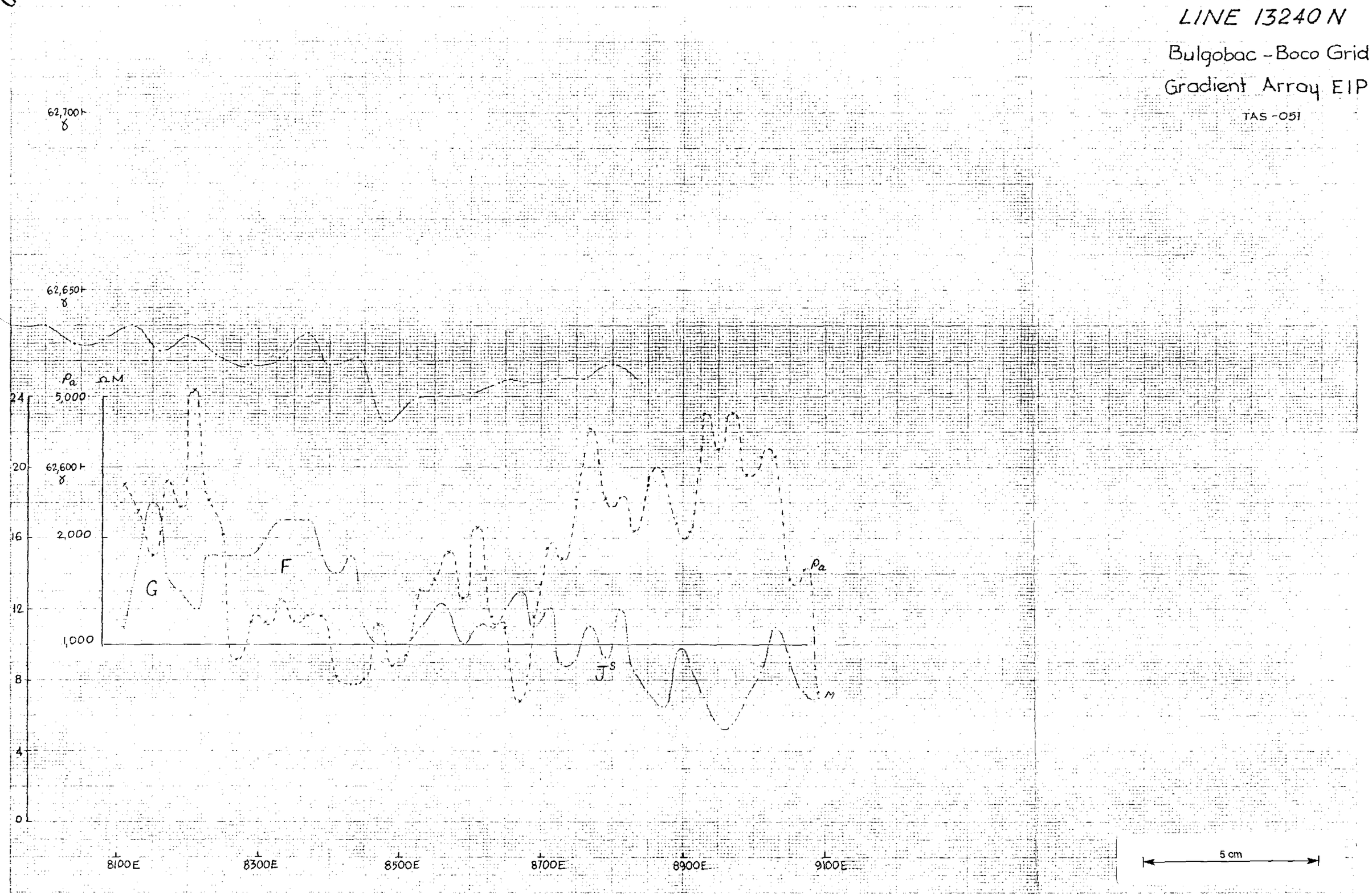

255052

LINE 13080 N

Bulgobac - Boco Grid

Gradient Array EIP

TAS-051

051

62,700E

62,650E

ρ_a Ω-M

5,000

2,000

1,000

M

ms

20

16

12

8

4

0

62,600E

G?

F

J^S

ρ_a

M

8100E

8300E

8500E

8700E

8900E

9100E

5 cm

052

255053

LINE 12920 N

Bulgobac - Boco Grid

Gradient Array EIP

TAS-051

62,700 γ

62,650 γ

62,600 γ

ρ_a Ω-M

10,000

5,000

2,000

1000

M ms

16

12

8

4

0

ρ_a

M

E

8100E

8300E

8500E

8700E

8900E

9100E

5 cm

255054

LINE 12760 N

Bulgobac - Boco Grid

Gradient Array EIP

TAS - 051

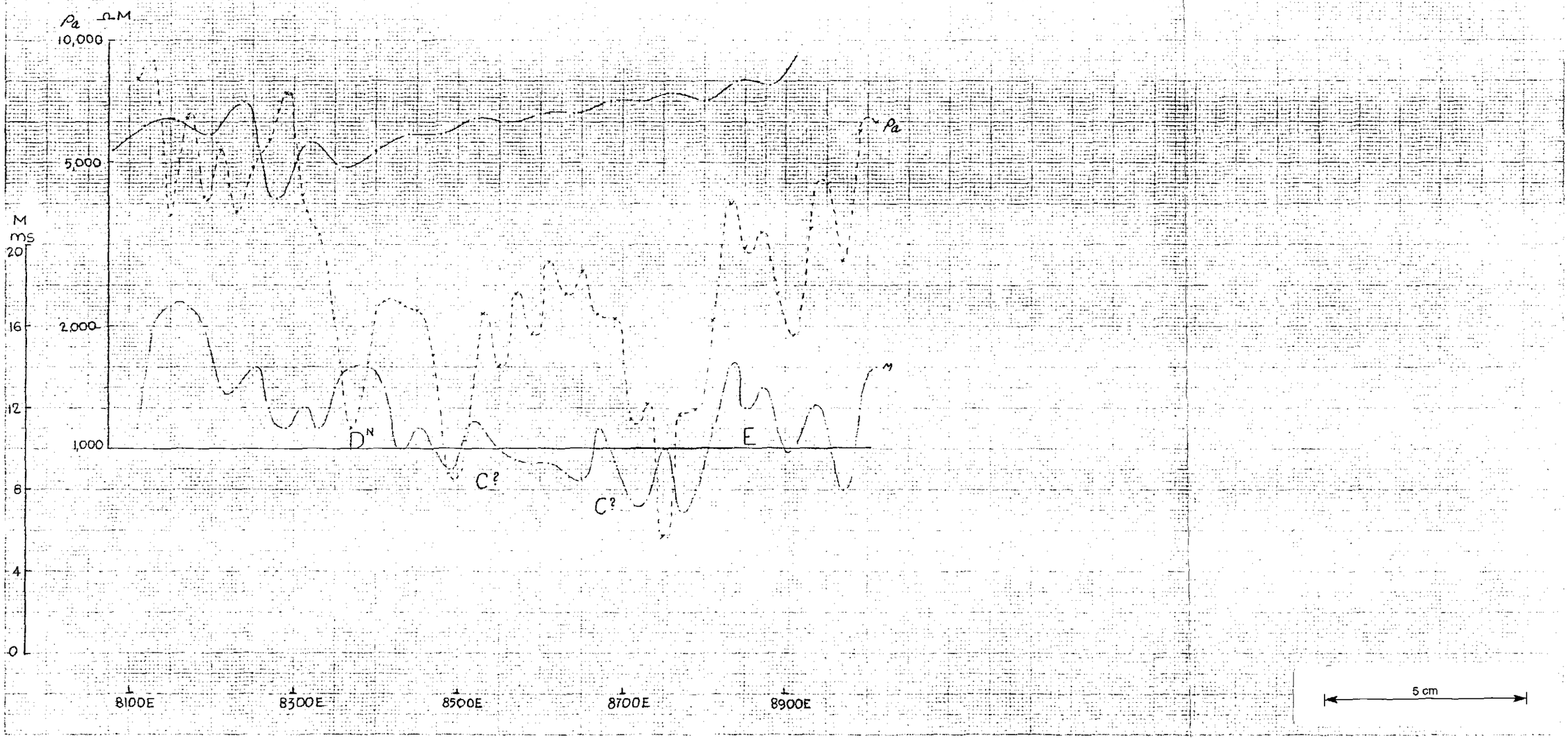

054

255055

LINE 12600 N

Bulgobac - Boco Grid

Gradient Array EIP

TAS-051

62,700 γ

62,650 γ

62,600 γ

ρ_a ΩM

10,000

5,000

2,000

1,000

N

MS

24

20

16

12

8

4

0

D^N

C

E

ρ_a

M

8300E

8500E

8700E

8900E

9100E

9300E

9500E

5 cm

255056

055

LINE 12280N

Bulgobac - Boco Grid

Gradient Array - EIP

TAS-051

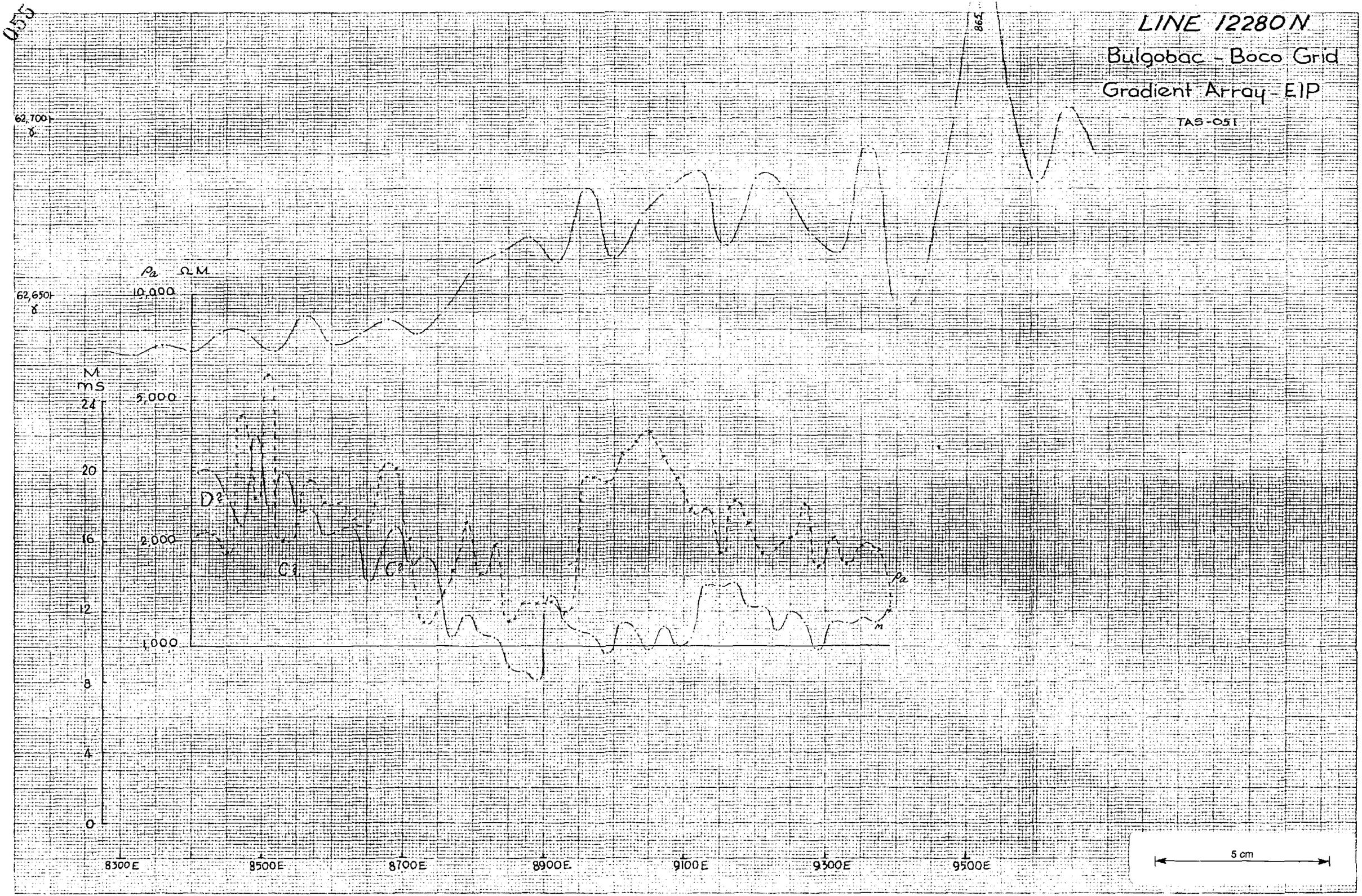

255057

LINE 12120 N

Bulgobac - Boco Grid

Gradient Array EIP

TAS-051

056

756 772 759

62,700 γ

62,650 γ

62,600 γ

ρ_a Ω M

10,000

5,000

2,000

1,000

M ms

20 16 12 8 4 0

A B

8300E 8500E 8700E 8900E 9100E 9300E 9500E

5 cm

255058

LINE 11960 N

Bulgobac - Boco Grid

Gradient Array - EIP

TAS-051

057

712 775 844 636 908 65019 749 714 746

62,600 γ

62,550 γ

62,500 γ

62,450 γ

62,400 γ

ρa ΩM

10,000

5,000

2,000

1,000

M mS

24 20 16 12 8 4 0

ρa

D5

NO SY

A B

M

8300E 8500E 8700E 8900E 9100E 9300E

5 cm

053

255059

LINE 11640N

Bulgobac - Boco Grid

Gradient Array-EIP

TAS-051

63033 746 786 858 775 820 839 857

62,700 γ

62,650 γ

62,600 γ

62,550 γ

ρ_a Ω-M

10,000

5,000

2000

1,000

M mS

24

20

16

12

8

4

0

D^S

NOISY

A

B

ρ_a

8300E 8500E 8700E 8900E 9100E 9300E 9500E

5 cm

1819

382 000E
383 000E
384 000E
385 000E

5 390 000 N
5 389 000 N
5 388 000 N

EMU BAY RAILWAY

MURCHISON HIGHWAY

E L 12/72

E L 12/72

XXII
XXI
XX

255060

5 cm

ELECTROLYTIC ZINC CO. OF A'ASIA. LTD

PROJECT BULGOBAC E.L 12/72 TAS.

CORRECTED BOCO GRID SHOWING

CHARGEABILITY CONTOUR PLAN

(IN MILLISECONDS)

Surveyed & Compiled by SCINTREX Pty Ltd. APRIL-JUNE 76

BOCO NORTH SHEET

SCALE 1 5 000

REFERENCE

REF. NO.

DATE 8/9/76 DRAWN R.A.H GEOLOGY N.H.H

PLATE 8

REVISED OCT 1977
JOB # TAS-051

SCINTREX SHT 1 of 3 PLATE 1

SCINTREX PTY, LTD, SHEET 1 OF 2 PLATE 4

78-1271 Vol. 2|2 . 1819

1820

78-1271 Vol. 2/2.

1820

1821

377 000E
378 000E
379 000E
380 000E

5 386 000N
5 385 000N
5 384 000N

8165E
7860E
8280E
8190E
8580E
8360E
8540E

E.L. 12 / 72
E.L. 12 / 72

PINNACLES SHEET
255062

5 cm

ELECTROLYTIC ZINC CO. OF A'ASIA. LTD.

PROJECT: BULGOBAC E.L.12/72 TAS.

CORRECTED BOCO GRID SHOWING

CHARGEABILITY CONTOUR PLAN

(IN MILLISECONDS)

BOCO SOUTH SHEET

Surveyed & Compiled by SCINTREX Pty Ltd. OCT 1977

SCALE: 1 : 5 000

REFERENCE:

REF. NO.

DATE: 1/2/78 DRAWN: R.A.H. GEOLOGY: N.H.H.

Job # TAS-081
SCINTREX PTY. LTD. SHEET 3 OF 3 PLATE 1

78-1271 Vol 2/2

1321

382 000E
383 000E
384 000E
385 000E
5 390 000 N
5 389 000 N
5 388 000 N
EMU BAY RAILWAY
MURCHISON HIGHWAY
E.L 12/72
E.L 12/72
X SX #3
5cm
255063
ELECTROLYTIC ZINC CO. OF A'ASIA. LTD
PROJECT: BULGOBAC E.L 12/72 TAS.
CORRECTED BOCO GRID SHOWING
RESISTIVITY CONTOUR PLAN
(IN OHM METRES)
BOCO NORTH SHEET
Surveyed & Compiled by SCINTREX Pty Ltd. APRIL-JULY
SCALE: 1: 5 000
REFERENCE
REF NO.
DATE 8/9/76 DRAWN R.A.H GEOLOGY N.H.H
PLATE 10
REVISED OCT 1977
JOB # TAS-051
SCINTREX SHT 1 of 3
PLATE 2
SCINTREX PTY. LTD.
SHEET 1 OF 2
PLATE 3
1822
79-1211 Vol. 2/2
1822

255064

5 cm

ELECTROLYTIC ZINC CO. OF A'ASIA LTD

PROJECT: BULGOBAC EL12/72 TAS

CORRECTED BOCO GRID SHOWING

RESISTIVITY CONTOUR PLAN

(IN OHM METRES)

BOCO SOUTH SHEET

Surveyed & Compiled by SCINTREX Pty Ltd. APRIL-JULY

SCALE 1 5 000 REF. NO.

REFERENCE

DATE 8/9/76 DRAWN R.A.H. GEOLOGY N.H.H. PLATE 11

REVISED OCT 1977

JOB # TAS-061 SCINTREX SHT 2 of 3 PLATE 2

SCINTREX PTY. LTD. SHEET 2 OF 2 PLATE 3

1823

78-1271 Vol. 2/2 .

1323

377 000E
378 000E
379 000E
380 000E

5 386 000N
5 385 000N
5 384 000N

8165E?
7860E ?
8280E?
8190E ?
8360E

E.L. 12 / 72
E.L. 12 / 72

PINNACLES SHEET
255065

5 cm

ELECTROLYTIC ZINC CO. OF A'ASIA. LTD.

PROJECT: BULGOBAC E.L 12/72 TAS.

CORRECTED BOCO GRID SHOWING

RESISTIVITY CONTOUR PLAN

(IN OHM METRES)

Surveyed & Compiled by SCINTREX Pty Ltd OCT 1977

SCALE: 1 : 5 000 REF. NO

REFERENCE:

DATE: 1/2/78 DRAWN: R.A.H. GEOLOGY N.H.H.

Job # TAS-051
SCINTREX PTY LTD SHT 3 of 3 PLATE 2

1824

78-1271 Vol. 2&2.

1824

382 000E
383 000E
384 000E
385 000E
5 390 000 N
5 389 000 N
5 388 000 N
EHL
BAY
RAILWAY
MURCHISON
HIGHWAY
Add 62.000 to all values.
E.L.12/72
E.L.12/72
5 cm
255066
ELECTROLYTIC ZINC CO. OF A'ASIA. LTD.
PROJECT: BULGOBAC E.L.12/72 TAS.
CORRECTED BOCO GRID SHOWING
TOTAL MAGNETIC FIELD CONTOUR PLAN
(IN GAMMAS)
BOCO NORTH SHEET
Compiled by SCINTREX Pty Ltd SEPT-OCT
SCALE: 1:5 000
REFERENCE:
REF. NO.
DATE 8/9/76 DRAWN R.A.H. GEOLOGY N.H.H.
PLATE 12
REVISED OCT. 1977
JOB # TAS-031
SCINTREX SHT 1 of 3
PLATE 3
SCINTREX PTY. LTD.
SHEET 1 OF 2
PLATE 5
1825
79-1271 Vol. 2/2
1325

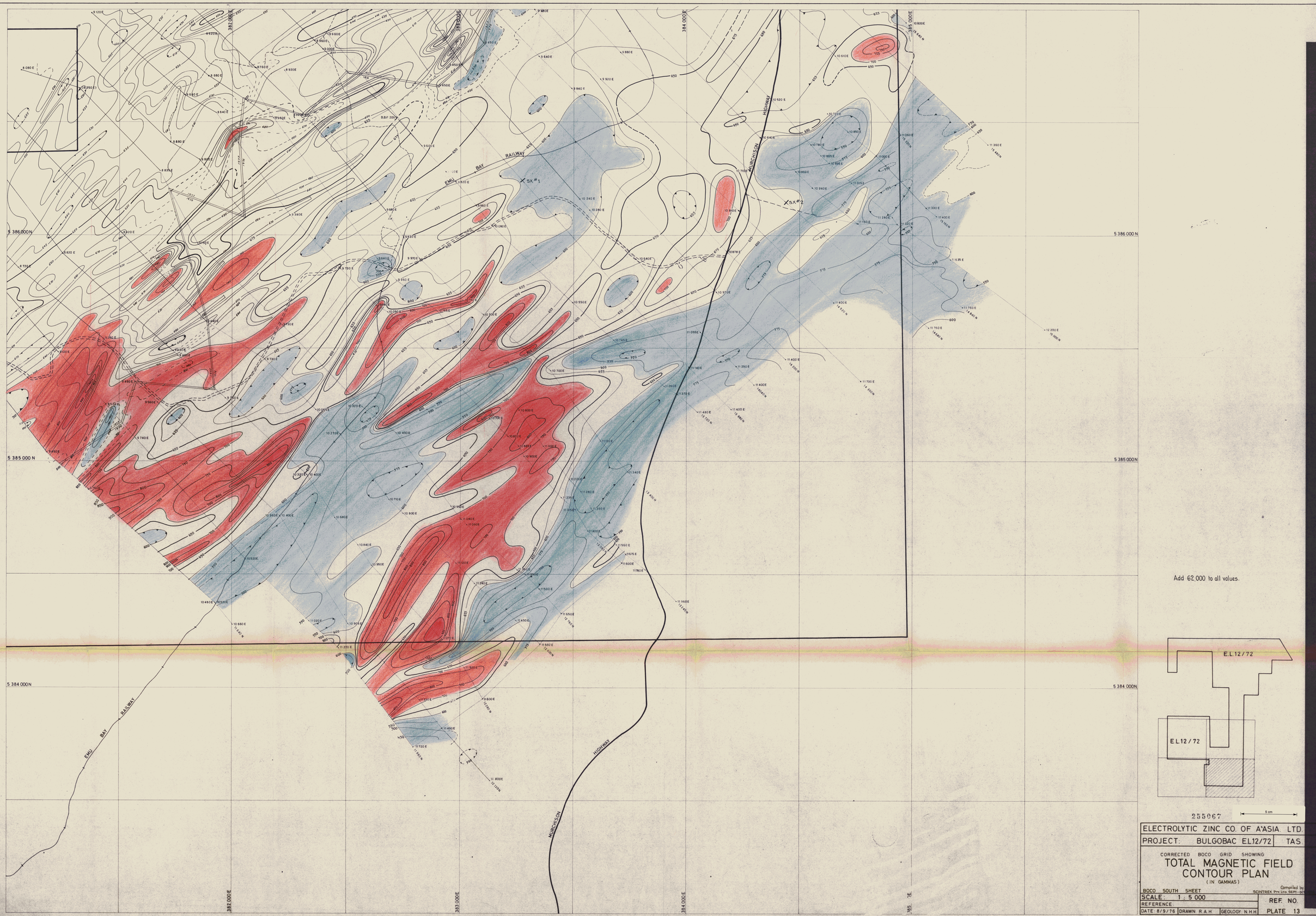

Add 62,000 to all values.

255067

5 cm

ELECTROLYTIC ZINC CO. OF A'ASIA. LTD.	
PROJECT: BULGOBAC EL12/72	TAS.

CORRECTED BOCO GRID SHOWING

TOTAL MAGNETIC FIELD CONTOUR PLAN

(IN GAMMAS)

Compiled by SCINTREX Pty Ltd. SEPT-OCT

BOCO SOUTH SHEET	
SCALE: 1 : 5 000	REF. NO.
REFERENCE:	PLATE 13
DATE: 8/9/76 DRAWN R.A.H. GEOLOGY N.H.H.	

REVISED OCT 1977 Job # TAS-051 — SCINTREX SHT 2 of 3 — PLATE 3

SCINTREX PTY. LTD. — SHEET 2 OF 2 — PLATE 5

1826

78-1271 Vol 2/2

1826

377 000E

378 000E

379 000E

380 000E

5 386 000N

5 385 000N

5 384 000N

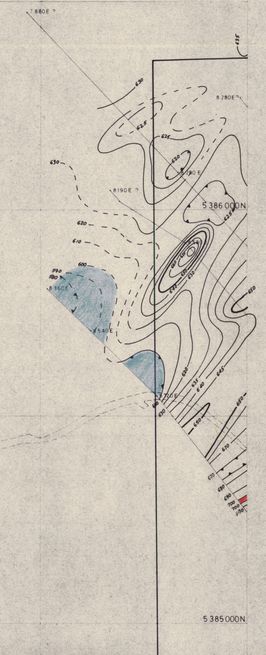

E.L. 12/72

E.L. 12/72

PINNACLES SHEET
255068

5 cm

ELECTROLYTIC ZINC CO. OF A'ASIA. LTD.

PROJECT: BULGOBAC E.L. 12/72 TAS.

CORRECTED BOCO GRID SHOWING

TOTAL MAGNETIC FIELD CONTOUR PLAN
(IN GAMMAS)

BOCO NORTH SHEET

Compiled by SCINTREX Pty Ltd OCT 1977

SCALE 1 5 000

REF NO

REFERENCE

DATE 1/2/78 | DRAWN: R.A.H. | GEOLOGY: N.H.H.

SCINTREX PTY. LTD. SHEET 3 of 3 PLATE 3

1827

78-1271 Vol 2/2

1827

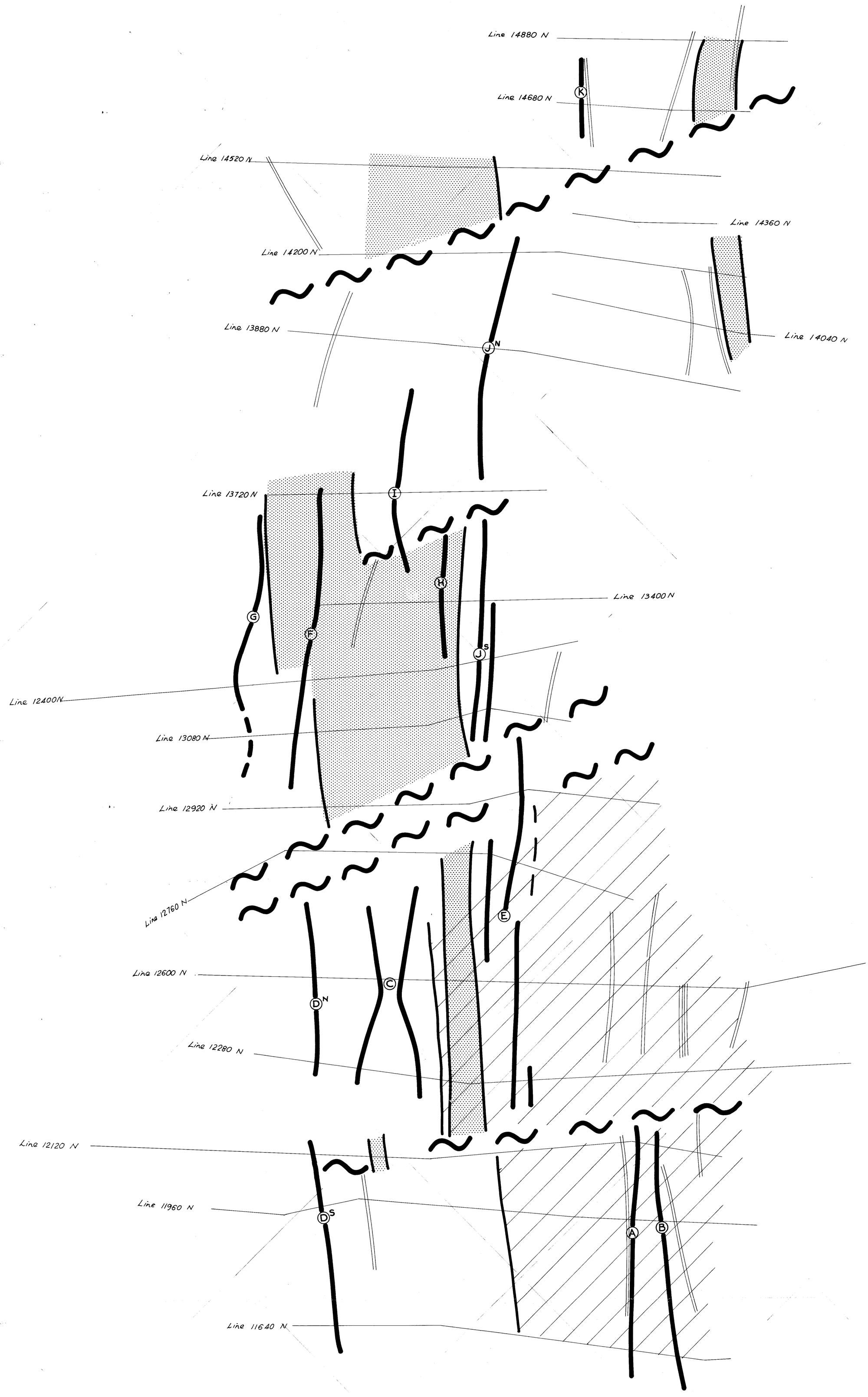

ELECTROLYTIC ZINC CO. OF A'ASIA LTD.

BOCO GRID

BULGOBAC E.L. 12/72 TASMANIA

GRADIENT ARRAY
ELECTRICAL INDUCED POLARIZATION
&
TOTAL MAGNETIC FIELD SURVEY

INTERPRETATION PLAN

ZONES OF LOW BACKGROUND RESISTIVITY

ZONES OF HIGHER TOTAL MAGNETIC FIELD BACKGROUND

AXIS OF MAGNETIC FIELD

(E) INDUCED POLARIZATION HIGHS

DISLOCATIONS

Grid N

SURVEYED & COMPILED BY
SCINTREX

OCTOBER 1977

255069

SCALE 1:5000

5 cm

Job. No. TAS-051 Sht 1 of 1 PLATE 4

78-1271 Vol. 2R

1328